

B. Siemon, A. Ullmann, I. Mitreiter
M. Ibs-von Seht, W. Voß, J. Pielawa



Bundesanstalt für
Geowissenschaften
und Rohstoffe

Airborne Geophysical Investigations of CLIWAT Pilot Areas

Survey Area Perkpolder, The Netherlands, 2009



Interreg IVB Project:
CLIWAT – Adaptive and sustainable
water management and protection of
society and nature in an extreme climate





**Bundesanstalt für Geowissenschaften und Rohstoffe
Federal Institute for Geosciences and Natural Resources**



**CLIWAT – Adaptive and sustainable water management and
protection of society and nature in an extreme climate
Survey Area Perkpolder, The Netherlands
2009**

Technical Report on the Interreg IVB Project



The project is part-financed by
the European Union

**In Cooperation with
TNO
Deltares**

**Authors: B. Siemon
A. Ullmann
I. Mitreiter
M. Ibs-von Seht
W. Voß
J. Pielawa**

Date: May 25, 2011

Table of contents

Personnel	III
List of figures	IV
List of tables	V
List of maps	VI
List of vertical resistivity sections	VII
Abbreviations	VIII
1. Summary	1
2. Introduction	3
3. Survey Area	6
4. Airborne Geophysical System	8
4.1. The Helicopter.....	9
4.2. Measuring System.....	9
4.3. Electromagnetics.....	10
4.4. Magnetics	11
4.5. Radiometrics	12
4.6. Navigation and Positioning.....	13
4.7. Data Acquisition and Recording.....	15
4.8. Video System.....	15
4.9. Additional Equipment	16
5. Processing and Presentation of the Survey Data	17
5.1. General Processing Steps.....	17
5.2. Position Data.....	18
5.2.1. Coordinates.....	18
5.2.2. Elevation	18
5.2.3. Radar Altitude.....	18
5.2.4. Laser Altitude.....	18
5.2.5. Topographic Elevation	19
5.3. Processing of the Electromagnetic Data.....	20
5.3.1. Calibration of the HEM System	20
5.3.2. Zero-Level and Drift Correction	21
5.3.3. Data Correction	21
5.3.4. Conversion of the Secondary Field Values to Half-Space Parameters	22

5.3.5. Effect of Anthropogenic Influences on the HEM Data.....	24
5.3.6. Statistical Levelling.....	25
5.3.7. 1-D Inversion of the HEM Data.....	27
5.3.8. Presentation of the Results.....	28
5.4. Processing of Magnetic Data.....	29
5.4.1. Magnetic Total Field.....	29
5.4.2. IGRF	29
5.4.3. Diurnal Variations	29
5.4.4. Levelling.....	29
5.4.5. Presentation of the Results.....	30
5.5. Processing of Gamma-Ray Spectrometry Data	31
5.5.1. Energy Calibration.....	31
5.5.2. Reduction of Statistical Noise.....	32
5.5.3. Detector Height above Ground and Effective Height.....	32
5.5.4. Live Time Correction.....	33
5.5.5. Background Radiation Correction	33
5.5.6. Compton Correction.....	34
5.5.7. Height-Attenuation Reduction	34
5.5.8. Radioelement Concentrations and Exposure Rate	35
5.5.9. Data Levelling and Smoothing.....	36
5.5.10. Presentation of the Results.....	36
6. Cartographic Work.....	37
6.1. Topographic Map.....	37
6.2. Map Production with GEOSOFT and GIS Software.....	37
6.3. Thematic Maps.....	38
7. Archiving	39
8. References	40
Signatures.....	41
Appendix I: Survey Area Perkpolder	42
Appendix II: Final Data Format Description	44
Appendix III: DVD	55
Appendix IV: Maps	58
Appendix V: Vertical Resistivity Sections	88

Personnel

Field Crew

Dr. Bernhard **Siemon**, project leader, operating and field data processing, B2.1, BGR

Angelika **Ullmann**, project scientist, field data processing, B2.1, BGR

Wolfgang **Vofß**, navigation, B2.1, BGR

Josef **Scheiwein**, helicopter engineering, B2.1, BGR

Michael **Schütt**, pilot, Wiking Helikopter Service GmbH

Office Crew

Dr. Uwe **Meyer**, leader of sub-department B2.1, BGR

Dr. Bernhard **Siemon**, project leader, electromagnetic data evaluation, B2.1, BGR

Angelika **Ullmann**, project scientist, electromagnetic data evaluation, B2.1, BGR

Ivonne **Mitreiter**, project scientist, electromagnetic data evaluation, B2.1, BGR

Dr. Malte **Ibs-von Seht**, magnetic and radiometric data evaluation, B2.1, BGR

Jens **Pielawa**, cartographic work, B2.1, BGR

Address: Federal Institute for Geosciences and Natural Resources (BGR)
Stilleweg 2
30655 Hanover
Germany
Tel.: +49 511 643 3212 (Meyer)
3488 (Siemon)
Fax: +49 511 643 3662
Email: Uwe.Meyer@bgr.de, Bernhard.Siemon@bgr.de

List of figures:

1. Regions funded by the Interreg IVB North Sea Region Programme
2. Perkpolder survey area
3. Principal sketch of the BGR airborne geophysical system
4. HEM inversion based on a homogeneous half-space or a layered half-space
5. Construction of starting models

List of tables:

1. Survey parameters for the Perkpolder survey area
2. Technical specifications of the BGR helicopter D-HBGR
3. The geophysical survey systems
4. HEM system parameters (Bird 61)
5. Base stations
6. Radiation sources and corresponding spectrometer parameters
7. Navigation and positioning systems
8. Altimeters
9. Data acquisition and recording systems
10. Video system
11. Additional equipment
12. Calibration factors of the HEM systems
13. Filter parameters for HEM data processing
14. Filter parameters for semi-automatic correction of man-made effects
15. Filter parameters for the levelling of HEM data
16. Filter parameters for levelled HEM data
17. Aircraft background and cosmic stripping factors
18. Stripping ratios
19. Height attenuation coefficient
20. Sensitivity coefficients
21. Coordinates of the corners of the 1:25,000 Perkpolder topographic map sheets
22. Grid parameters
23. Content of the DVD

A-1 Flight table

List of maps:

1. Flight lines,
2. Digital elevation model,
3. Apparent resistivity at 133,300 Hz (rhoa6),
4. Apparent resistivity at 41,440 Hz (rhoa5),
5. Apparent resistivity at 8,395 Hz (rhoa4),
6. Apparent resistivity at 5,407 Hz (rhoa3),
7. Apparent resistivity at 1,821 Hz (rhoa2),
8. Apparent resistivity at 387 Hz (rhoa1),
9. Centroid depth at 133,300 Hz (zst6),
10. Centroid depth at 41,440 Hz (zst5),
11. Centroid depth at 8,395 Hz (zst4),
12. Centroid depth at 5,407 Hz (zst3),
13. Centroid depth at 1,821 Hz (zst2),
14. Centroid depth at 387 Hz (zst1),
15. Resistivity at 01 m bsl,
16. Resistivity at 02 m bsl,
17. Resistivity at 04 m bsl,
18. Resistivity at 07 m bsl,
19. Resistivity at 10 m bsl,
20. Resistivity at 13 m bsl,
21. Resistivity at 16 m bsl,
22. Resistivity at 20 m bsl,
23. Depth to salt water in m bgl,
24. Anomalies of the total magnetic field (ΔT),
25. Concentration of Potassium (K),
26. Equivalent concentration of Thorium (Th),
27. Equivalent concentration of Uranium (U),
28. Stripped total count rate (TC),
29. Ground level exposure rate in $\mu R/h$.

List of vertical resistivity sections:

Tie lines:

1. VRS 1.9
2. VRS 2.9
3. VRS 3.9
4. VRS 4.9
5. VRS 5.9
6. VRS 6.9
7. VRS 7.9
8. VRS 8.9
9. VRS 9.9
10. VRS 10.9,
11. VRS 11.9,
12. VRS 12.9,
13. VRS 13.9

Lines:

14. VRS 1.1,
15. VRS 2.1,
16. VRS 3.1,
17. VRS 4.1,
18. VRS 5.1,
19. VRS 6.1,
20. VRS 7.1,
21. VRS 8.1,
22. VRS 9.1,
23. VRS 10.1,
24. VRS 11.1,
25. VRS 12.1,
26. VRS 13.1,
27. VRS 14.1,
28. VRS 15.1,
29. VRS 16.1,
30. VRS 17.1,
31. VRS 18.1,
32. VRS 19.1,
33. VRS 20.1,
34. VRS 21.1,
35. VRS 22.1

Five and fifteen layer models were calculated for all sections.

Abbreviations

°	degree
°C	degree Celsius
'	minute
"	second or inch
%	per cent
1-D	one-dimensional
a	aircraft background
A	amplitude of measured HEM components
A_c, A'_c	amplitudes of calculated HEM components
A'_p	polynomial approximation of $A'_c(\delta)$
Ah	ampere hours
agl	above ground level
asl	above mean sea level
α, β, γ, a	stripping ratios
$\alpha_e, \beta_e, \gamma_e$	height corrected stripping ratios
α_0	complex wave number
b	cosmic stripping factor
bgl	below ground level
BGR	Bundesanstalt für Geowissenschaften und Rohstoffe
Bi	Bismuth
B_n	layer admittance
bsl	below sea level
C	concentration
C_0	element concentration at ground
C_H	element concentration in presence of vegetation
CF	compact flash
ch	channel number
c_l	effective cable length
cps	counts per second
Cs	Caesium
©	copyright
d_a	apparent depth
D_a	apparent distance
DC	direct current
DEM	digital elevation model
DGPS	Differential Global Positioning System
DK	Denmark
D_s	depth to salt water
DVD	Digital Versatile Disc
δ	inverse relative skin depth (= h/p)

δ_p	polynomial approximation of $\delta(\epsilon_c)$
δ_T	residual (magnetics)
ΔI	zero-level error of in-phase component
ΔQ	zero-level error of quadrature component
ΔT	anomalies of the total magnetic field
ΔV	diurnal (magnetic) variations
E	east
E	energy
E	ground level exposure rate
e	base of the natural logarithm ($1/e \approx 0.37$)
eTh	equivalent concentration of Thorium
eU	equivalent concentration of Uranium
EM	electromagnetic(s)
ERDF	European Regional Development Fund
EU	European Union
ϵ	ratio of measured HEM components (= Q/I)
ϵ_c	ratio of calculated HEM components (= Q/I)
ϵ_0	permittivity of air: 8.854×10^{-12} As/Vm
ϵ_n	layer permittivity
f	frequency
F	IRGF
FAS	Fugro Airborne Surveys
FFT	Fast Fourier Transform
ft	feet
G	gain constant
GBA	Geologische Bundesanstalt
GPS	Global Positioning System
h	bird altitude
HCP	horizontal coplanar
h_e	effective height
h_0	nominal survey height
HEM	helicopter-borne electromagnetic(s)
HMG	helicopter-borne magnetic(s)
HRD	helicopter-borne radiometric(s)
h_GPS	GPS elevation of the bird
h_GPS_heli	GPS elevation of the helicopter
h_l	laser altitude
h_r	radar altitude of the bird
h_r_heli, h_r	radar altitude of the helicopter
Hz	hertz
i	counter

I	in-phase component (real part) of the HEM data
I_c	calculated in-phase value
IAEA	International Atomic Energy Association
IAGA	International Association of Geomagnetism and Aeronomy
IGRF	International Geomagnetic Reference Field
J_0	Bessel function of first kind and zero order
K	degree Kelvin
K	Potassium
keV	kilo electron volts
kg	kilogram
kHz	kilohertz
km	kilometre
km/h	kilometres per hour
l	litre
log	logarithm
λ	wave number
m	metre
MeV	mega electron volts
μ	attenuation coefficient
μ_0	permeability of air: $4\pi \times 10^{-7}$ Vs/Am,
μ_n	layer permeability
μ R/h	microrentgens per hour
n	number of frequencies
N	north
n, N	raw, corrected count rate
NaI	sodium iodide
NASVD	noise adjusted singular value decomposition
NL	non-linear
NL	The Netherlands
nT	nanotesla
N_m'	observed count rate at STP effective height
N_s	corrected count rate at nominal survey height
N_x	background and STP corrected count rates (x = K, U, Th)
$N_{x(\text{corr})}$	stripping corrected count rates (x = K, U, Th)
Ω m	ohm metre (Ohm*m)
p	skin depth
P	barometric pressure
P_0	barometric pressure at sea level
PDF	Portable Document Format
ppm	parts per million
π	Pi (=3.14159265...)

Q	quadrature or out-of-phase component (imaginary part) of the HEM data
Q_c	calculated quadrature value
r	distance parameter
R_1	reflexion factor
r_1	conversion factor
ρ	resistivity
ρ_0	resistivity of air: $> 10^8 \Omega\text{m}$
ρ_a	apparent resistivity
S	south
S	sensitivity
s	second
STE	standard error
STP	standard pressure and temperature
t	thickness (of a model layer)
t	time variable
T	air temperature
T_0	temperature at freezing point of water on Kelvin scale
T, TMI	total magnetic field intensity
tanh	hyperbolic tangent
TC	total count rate
Th	Thorium
Tl	Thallium
t_l	life time
T_{LP}	low pass cut-off period
U	Uranium
USA	United States of America
USB	Universal Serial Bus
UTC	Coordinated Universal Time
UTM	Universal Transverse Mercator Projection
V	volt
VCX	vertical coaxial
VRS	vertical resistivity section
W	west
WFD	Water Framework Directive
WGS	World Geodetic System
ω	circular frequency
X, Y, Z	Cartesian coordinates, Z depth axis
Z	relative secondary magnetic field
z^*	centroid depth

1. Summary

Climate change simulations indicate a sea-level rise and increasing rainfall in the North Sea region leading to higher groundwater levels and a forced outwash of nutrients and pollutants from industrial areas, agriculture and landfills. CLIWAT (climate & water) is a transnational Interreg project in the North Sea region funded by the European Union with partners from Belgium, The Netherlands, Germany and Denmark. The goal of the project is to determine the effects of a possible climate change on groundwater systems, surface water and the freshwater/salt-water boundary in the North Sea and Baltic Sea region.

Geological and geophysical measurements were carried out in the seven pilot areas of the project. In order to map the existing groundwater structures with airborne geophysical methods the German Federal Institute for Geosciences and Natural Resources (BGR) conducted four surveys in Zeeland, Friesland (both NL) and Vojens (DK). One of these pilot areas covers parts of Zeeland. The aim of the airborne survey in this pilot area was to map the depth to the salt water in order to outline the thickness of freshwater saturated sediments of a fossil creek.

By request of the Dutch project partners (Deltares/TNO) a helicopter-borne survey of the area near Kloosterzande in Zeeland was conducted by the BGR airborne group in August 2009. The airborne survey comprises a 7 km by 7 km wide area ranging from 3°57'E to 4°03'E and 51°22'N to 51°25'N. With 2 survey flights 22 E–W profile lines and 13 N–S tie lines were flown, totalling about 214 line-km. The nominal flight-line spacing was 200 m for the profile lines and 500 m for the tie lines.

The BGR helicopter-borne geophysical system includes six-frequency electromagnetics (HEM), magnetics (HMG) and radiometrics (HRD). The electromagnetic system provides information about the distribution of electrical conductivity in the earth down to a maximum depth of 150 m. The intensity of the earth's total magnetic field is measured with a magnetometer. Magnetic anomalies may have deep sources as well as shallow ones. The intensity of the gamma radiation is registered by a gamma-ray spectrometer. The radiation measured is mainly emitted from the elements thorium, uranium, and potassium. The origin of this radiation is normally close to the earth's surface.

The helicopter-borne system consists of the BGR helicopter, the geophysical equipment and electronic equipment for navigation. The HEM and HMG sensors, a GPS antenna and a laser altimeter are installed inside a towed tube, called bird. The navigation instruments and the gamma-ray spectrometer are mounted in the helicopter. A ground base station records the time-variant data required to correct the airborne data.

The survey altitudes of the sensors are normally 30–40 m for electromagnetics and magnetics and 70–80 m for gamma-ray spectrometry. HEM and HMG data are recorded 10 times per second during a survey flight and HRD data are recorded once per second. At an aircraft speed of about 140–150 km/h, this leads to mean sampling intervals of about 4 m and 40 m, respectively.

The collected geophysical data and the corresponding positioning data are stored on a CF card during the flight. The digital data are checked immediately after the flight. Further processing of all survey data, including the data of the simultaneously operating base station which records the variations of

the total magnetic intensity and the variations of the atmospheric pressure, take place in the field and finally at BGR in Hanover.

This “Technical Report” describes the survey operations and the survey equipment used, as well as the data processing and the presentation of the results as vertical resistivity sections and thematic maps. The processed data, the thematic maps and the vertical sections are stored on a DVD, accompanying this report.

Following parameters are displayed on a topographic map at a scale of 1:25,000:

- actual flight lines,
- topographic elevations,
- apparent resistivities at six frequencies (387, 1,821, 5,407, 8,395, 41,440 and 133,300 Hz),
- centroid depths at six frequencies (387, 1,821, 5,407, 8,395, 41,440 and 133,300 Hz),
- resistivities at 1, 2, 4, 7, 10, 13, 16 and 20 m below sea level,
- depth to salt water in m below ground level,
- anomalies of the total magnetic field,
- concentration of potassium,
- equivalent concentration of thorium,
- equivalent concentration of uranium,
- total count rate,
- exposure rate.

Cross-sections based on resistivity-depth 1-D inversion models (vertical resistivity sections) are displayed along all flight lines at a horizontal scale of 1:25,000 with a vertical exaggeration of 25.

2. Introduction

Climate change simulations indicate a sea-level rise and increasing rainfall in the North Sea region. This will lead to higher groundwater levels and a forced outwash of nutrients and pollutants from industrial areas, agriculture and landfills (<http://cliwat.eu/>). The climate changes will affect the assessment of suitable industrial and agricultural development areas due to changes in the shape of the local waterworks catchments areas. Rise in groundwater level will challenge the construction business and it will be necessary to come up with new standards. It will also change the available groundwater resource and pattern of stream flow between summer and winter (reduced potential for irrigation from water table aquifers interacting with streams).

CLIWAT (climate & water) is a transnational project funded by the Interreg IVB North Sea Region Programme of the European Regional Development Fund (ERDF) with partners from four participating countries of the European Union (EU): Belgium (Ghent University), The Netherlands (Deltares/TNO, VITENS, Provincie Fryslân, Wetterskip Fryslân), Germany (LIAG, LLUR, SEECON, BGR) and Denmark (Region Midtjylland, GEUS, Region Syddanmark, Environment Centre Aarhus, Environment Centre Ribe, Aarhus University, Municipality of Horsens).

The goal of the project is to determine the effects of a possible climate change on groundwater systems, surface water and the freshwater/salt-water boundary in the North Sea and Baltic Sea region. The effect of the increased flux from agricultural and industrial land sites and landfills on groundwater quality in relation to indicators in the EU Water Framework Directive (WFD) has to be investigated as well as the impact on waterworks and important ground water aquifers near the coastlines. Also open question are the potential towards more accessible water in the hydrological system, the assessment of the consequences due to the increased recharge to groundwater systems and how to manage and solve the upcoming challenges for the construction business, for drainage and changes in conditions for biological/chemical decomposition in the soil.

Therefore geological and geophysical measurements were carried out in the seven pilot areas of the project (**Fig. 1**):

- A: Belgische Middenkust, Belgium,
- B: Zeeland, The Netherlands,
- C: Terschelling and Northern Friesland, The Netherlands,
- D: Borkum, Germany,
- E: Schleswig and Southern Jutland, Germany and Denmark,
- F: Egebjerg, Denmark,
- G: Aarhus river, Denmark.

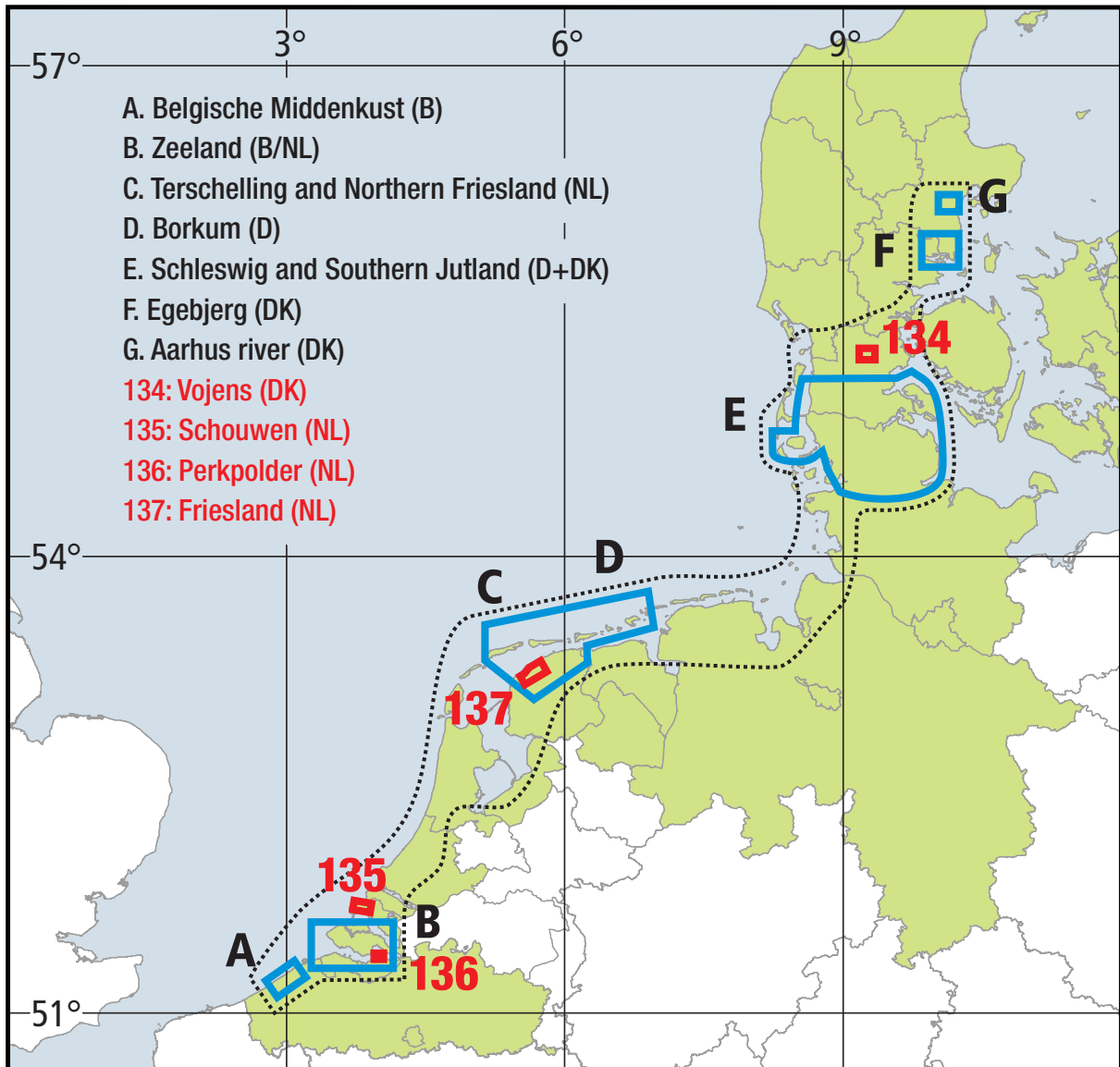


Fig. 1: Regions (green) funded by the Interreg IVB North Sea Region Programme of the European Regional Development Fund (ERDF) and project areas A-G. Red numbers indicate the BGR airborne survey areas.

One of these pilot areas (**B**) covers parts of Zeeland (**Fig. 2**). The aim of the airborne survey in this pilot area (136 Perkpolder) was to map the depth to the salt water in order to outline the thickness of freshwater saturated sediments of a fossil creek.

A helicopter-borne survey of the area near Kloosterzande was conducted by the BGR airborne group in August 2009. The Dutch project partners, who are responsible for the coordination of the measurements and the interpretation of the diverse data sets of the area, requested this airborne survey.

This “Technical Report” describes the survey operations and the survey equipment in use, as well as the data processing and the presentation of the results as vertical resistivity sections and thematic maps. The processed data, the thematic maps and the vertical sections are stored on a DVD accompanying this report.

3. Survey Area

The Perkpolder survey area near the town of Kloosterzande is bounded by a creek (De Vogel) in the south and by the Westerschelde in west, north and east. It comprises a nominally 7 km by 4 km wide area. The actual survey area ranging from 3°57'E to 4°03'E and 51°22'N to 51°25'N differs from the planned one as the tie lines were extended about 3 km to the south. A map of the projected survey area (small red dots) and its actual realization (bold red dots) is shown in **Fig. 2**, which also shows the boundary (dashed grey line) of the 1:25,000 topographic map used to present the geophysical results.

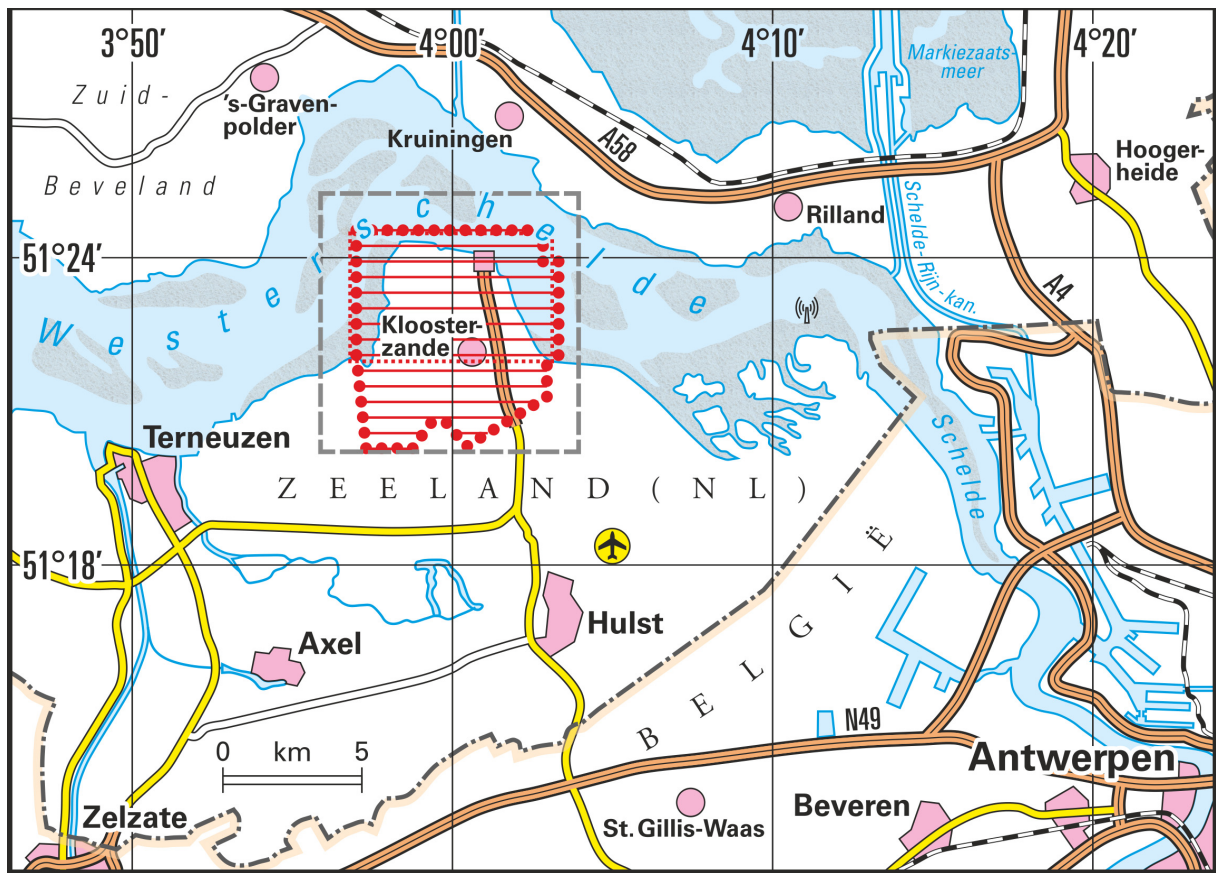


Fig. 2: Perkpolder survey area (bold red dots), projected area (red dotted line) and the frame of the map (grey dashed line).

An area of approximately 49 km² was surveyed with 2 survey flights on August 26–27, 2009. There were 22 E–W profile lines and 13 N–S tie lines flown, totalling about 214 line-km. The nominal flight-line spacing was 200 m for the profile lines and 500 m for the tie lines. The survey flights commenced from airport Midden Zeeland (2 m asl). The survey parameters are given in **Table 1**.

Table 1: Survey parameters for the Perkpolder survey area.

Survey area BGR area number	Perkpolder (NL) 136
Field period	August 26–27, 2009
Size of survey area	49 km ²
Total length of survey lines	214 km
Number of survey flights	2
Flight numbers	13601–13602
Mean flight altitude of the EM sensor above ground	38 m
Mean survey speed	135 km/h
Number of profile-line flights	1
Number of profile lines	22
Profile-line lengths	4–7 km
Profile-line directions (angle to N)	90°
Profile-line spacing	200 m
Number of tie-line flights	1
Number of tie lines	13
Tie-line lengths	4–8 km
Tie-line directions (angle to N)	0°
Tie-line spacing	500 m

The lines flown primarily northwards or eastwards are normally given an even profile number, while the ones flown in the opposite directions are odd numbered. The profile lines have the extension “.1” (after the profile number), and the tie lines have the extension “.9” or “.8” for repeated lines. Details of the survey flights are given in **Appendix I**.

The average altitude of the helicopter was 38 m above ground level within the survey area. During a survey flight, particularly before the first and after the last profile, the altitude was increased to >350 m to check the calibration of the HEM system far from any disturbing influences.

The base station recording the magnetic variations was located on the airport Midden Zeeland at 3°43'20"E, 51°30'48"N and 2 m asl.

4. Airborne Geophysical System

BGR's airborne geophysical system simultaneously records the electromagnetic, magnetic, and gamma-ray spectrometry data. The geophysical instrumentation, the navigation and positioning systems, the digital recording units, as well as other equipment needed for the survey flights are integrated in one measuring system carried by a Sikorsky S-76B helicopter (**Fig. 3**).

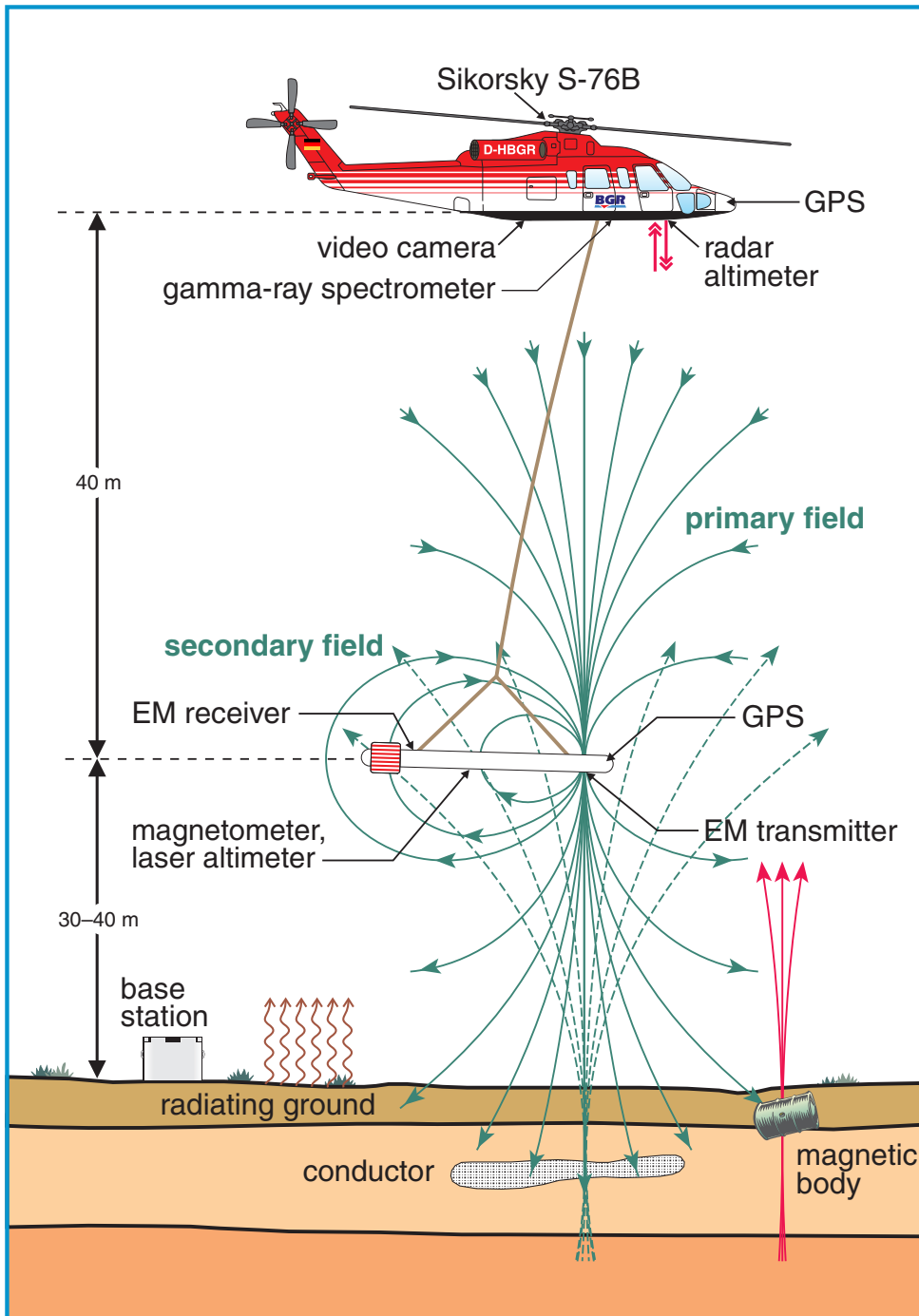


Fig. 3: Principal sketch of the BGR airborne geophysical system.

4.1. The Helicopter

The helicopter, a Sikorsky S-76B (see **Table 2**), was purchased in 1986 by the Federal Ministry for Economic Cooperation and Development and assigned to BGR, mainly for technical cooperation projects.

Table 2: *Technical specifications of the BGR helicopter D-HBGR*

Helicopter	
Type	Sikorsky S-76B (Manufacturer: Sikorsky, USA)
Year of manufacture	1986
Engines	2 turbines Pratt & Whitney PT6B-36A with 1033 SHP (shaft horse power) for each
Maximum gross weight	11,700 pounds (5,363 kg)
Maximum payload	3,300 pounds (1,500 kg)
Maximum flight duration	2:45 hours
Fuel consumption per hour	350–400 l

4.2. Measuring System

The airborne geophysical system (**Table 3**) is installed in the helicopter and in a towed tube, called bird. The navigation instruments and the gamma-ray spectrometer are mounted in the helicopter. The HEM and HMG sensors, a GPS antenna and a laser altimeter are installed inside the bird. This bird is towed by a 45 m long cable and its position is, depending on the flight speed, about 40 m beneath and little behind the helicopter. A ground base station records the time-variant data required to correct the airborne data.

The geophysical and recording systems are controlled by the HeliDas system that also assists navigation during a survey flight. The operator and the navigator are able to check the flight data online as information about the flight path and selected data channels are displayed on tablet computers.

Table 3: *The geophysical survey system*

Geophysical systems		
Bird	I. Six -frequency electromagnetic system (HEM)	
	Function	Investigation of the underground electric conductivity down to a maximum depth of about 150 m
	Manufacturer	Fugro Airborne Surveys (FAS), Canada
	Type	RESOLVE, BKS36a (Bird 61)
	II. Caesium magnetometer	
	Function	Recording of the total magnetic intensity of the earth
	Manufacturer	Geometrics, USA
Helicopter	Type	G-822A
	III. Gamma-ray spectrometer	
	Function	Recording of the energy spectrum of natural and man-made gamma radiation within a range of 0 to 3 MeV
	Manufacturer	Exploranium, Canada
Type	Spectrometer: GR-820; Detector crystals: GPX-1024/256	

4.3. Electromagnetics

A sinusoidal current flow through a transmitter coil at a discrete frequency generates the primary magnetic field. At a distance greater than about 2 m this field is very similar to a field of a magnetic dipole located in the centre of the transmitter coil. The resulting eddy currents in the subsurface generate a secondary magnetic field that depends on the frequency used and the conductivity distribution. The difference of the fields picked up by the receiver coil and a bucking coil, which is used to cancel out the dominating primary field, is related to the primary magnetic field at the receiver coil, i. e., the quantity measured is the relative secondary magnetic field in parts per million (ppm). Due to a small phase shift between the primary and the secondary field, the relative secondary magnetic field is a complex quantity with in-phase and out-of-phase (quadrature) components.

The HEM system (RESOLVE) manufactured by Fugro Airborne Surveys utilises six individual coil systems (**Table 4**) consisting of transmitter, receiver, bucking and calibration coils. The transmitter and receiver coils have a diameter of about half a metre and a distance of about 8 m. The orientation of five transmitter-receiver coil systems is horizontal coplanar (HCP) what is suitable for groundwater exploration purposes as the induced currents are predominantly flowing horizontally resolving layered structures best. In addition, a vertical coaxial coil (VCX) system is used in order to better locate vertical structures such as fault or fracture zones. The coil systems are housed by a 10 m long tube.

Table 4: HEM system parameters (Bird 61)

Frequency [Hz]	Coil separation [m]	Coil orientation	Denotation FAS	Denotation BGR
387	7.938	horizontal coplanar	EM_3	1. frequency
1,821	7.931	horizontal coplanar	EM_5	2. frequency
5,407	9.055	vertical coaxial	EM_6	3. frequency
8,395	7.925	horizontal coplanar	EM_2	4. frequency
41,440	7.912	horizontal coplanar	EM_1	5. frequency
133,300	7.918	horizontal coplanar	EM_4	6. frequency

Small coils placed in the centre of each receiver coil are used for calibration. The calibration factors necessary to convert the measured signals to ppm values were provided by the manufacturer. The in-phase and quadrature components of the relative secondary magnetic fields are used to derive the three-dimensional distribution of the electrical conductivity – or its inverse, the resistivity – in the subsurface. Horizontal resolution and vertical resolution are achieved by moving the system and using different system frequencies, respectively. Due to the skin-effect (high frequency currents are flowing on top of a perfect conductor) the penetration depths of the electromagnetic fields increase with decreasing frequency and conductivity. The frequencies used range from 387 Hz to 133 kHz enabling exploration depth ranges of about 1–30 m in a very conductive host such as salt-water saturated sediments and 5–150 m in a rather resistive host such as freshwater saturated sandy sediments.

The HEM system is not only sensitive to the electrically conductive subsurface but also to anthropogenic objects like, e. g., buildings, metallic bodies, and electrical installations, which have influence on the data measured, particularly at lower frequencies. As the helicopter itself is such an object, the HEM system is towed at a sufficiently large distance (about 40 m) underneath the helicopter.

4.4. Magnetics

A highly sensitive caesium vapour magnetometer installed in the bird is used to measure the total intensity of the earth's magnetic field (unit Nanotesla, nT). The function of a caesium magnetometer is based on the measurement of the Larmor frequency that occurs in a special, optically pumped system in the sensor. The frequency is directly proportional to the magnetic field intensity and can be determined with high precision and accuracy. The resolution of the instrument is 0.01 nT.

The magnetic field measured is composed of different parts. The earth's main field, caused by sources in the earth's core, varies between approximately 20,000 nT in equatorial regions and 70,000 nT at the poles. It is superimposed by the crustal magnetic field caused by rocks containing magnetised minerals. These produce anomalies in the range between less than one and up to several hundred nT. In populated areas, anthropogenic sources such as buildings, industrial plants, power

lines, etc. can produce additional locally confined and sometimes strong magnetic anomalies. Finally, the magnetic field is subject to temporal changes due to fluctuations in the state of the ionosphere and magnetosphere. These diurnal variations are in the order of several tens of nT.

In order to record the diurnal variations, a magnetic base station (**Table 5**) is operated. The station, also equipped with a caesium magnetometer, is installed close to the area of investigation at a magnetically undisturbed place. Data recorded by the base station during the survey are used to correct the total magnetic field measured during the flight. GPS time is used to synchronise both data sets.

Table 5: *Base station*

Base station	
Magnetic base station	
Function	Recording of the variation of the total magnetic intensity (TMI)
Manufacturer	Base station: FAS, Canada Magnetometer: Cs sensor H-8, SCINTREX, Canada
Type	CF1 Data Logger

4.5. Radiometrics

For geophysical investigations the count rates of the common terrestrial radioactive elements (or their isotopes and daughter products) Tl-208 (thorium series), Bi-214 (uranium series), K-40 (potassium) are of interest. Mapping of the distribution of these three elements in the ground are useful for geological investigations.

BGR uses a standard 256-channel spectrometer system consisting of four sodium iodide (NaI) crystals to detect the ground gamma radiation and one upward looking crystal to detect the radon radiation in the air. The spectrometer crystals are placed together in an aluminium box. Each crystal has a volume of approximately 4 l ($0.1 \times 0.1 \times 0.4 \text{ m}^3$). Incident gamma radiation is absorbed by the crystals and transformed to light pulses that are converted to electric pulses using a photomultiplier tube. The amplitudes of the electric pulses are directly proportional to the energy of incident gamma radiation.

The spectrometer covers an energy spectrum from 0 to 3 MeV. Depending on their energy, the pulses are mapped into one of 255 energy channels. Channel 256 is reserved for recording cosmic radiation between 3 and 6 MeV. Spectra recorded by the system contain counts of gamma radiation collected and integrated over one second. Energy windows and channel ranges of the different radiation sources are listed in **Table 6**. The spectrometer is internally stabilised for possible drifts in gain. This is done independently for each of the four downward-looking crystals using the thorium peak. Shifts of the thorium peak (2.62 MeV) relative to the nominal value are identified and the gain of the photomultiplier tube of the respective crystal is corrected automatically. A caesium sample is used to stabilize the gain of the upward looking crystal.

Table 6: Radiation sources and corresponding spectrometer parameters

Radiation source	Energy window in MeV	Peak energy in MeV	Channel range
Total count	0.41–2.81	—	34–233
Potassium (K-40)	1.37–1.57	1.46	115–131
Uranium (Bi-214)	1.66–1.86	1.76	139–155
Thorium (Tl-208)	2.41–2.81	2.62	202–233
Cosmic radiation	3.0–6.0	—	255

4.6. Navigation and Positioning

The navigation system (**Table 7**) provides the pilot with all the information necessary to carry out a survey flight. Navigation software (LiNav, AG-NAV Inc.) calculates the coordinates of the starting and the end points of all survey lines from the coordinates of the corners of the survey area, the profile direction and the spacing of the flight lines. These coordinates are copied to the HeliDas system using a CF card or an USB stick. These profiles are displayed on the tablet computer with the line being flown highlighted.

Table 7: Navigation and positioning systems

Systems for navigation and positioning		
Helicopter	Navigation system	
	Function	On-line determination and display of the GPS navigational data required by the pilot during a survey flight; recording of the geographic position of the helicopter and its altitude above mean sea level
	Manufacturer	Navigation computer and display: FAS, Canada GPS receiver: NovAtel, Canada
	Type	Navigation computer: HeliDas GPS receiver: NovAtel OEMV-2-L1/L2 GPS antenna: NovAtel L1/L2 ANT-532-e
Bird	Positioning system	
	Function	Determination and recording of the geographic position of the HEM bird and its altitude above mean sea level
	Manufacturer	Position recording and display: FAS, Canada GPS receiver: CSI Wireless, Canada
	Type	Position recording: HeliDas GPS receiver: DGPS MAX

The pilot obtains all information required to fly the profiles as accurately as possible from a second display. The most important information is the lateral deviation from a line. The deviation appears digitally in metres, as well as on a bar diagram. The navigation computer receives information about the position of the helicopter from a GPS navigation receiver whose antenna is fixed outside on the helicopter. The error in the navigation data is less than 1–2 m.

The positioning system (**Table 7**) provides the coordinates of each geophysical measurement. A second GPS navigation receiver is used for this purpose, whose antenna is fixed inside the bird. The spatial positions of the sensors are determined from this positioning data. The error of the coordinates is also in the order of 1–2 m.

A radar altimeter (**Table 8**) attached to the bottom of the helicopter determines its altitude above the ground or above obstacles (e. g., large stands of trees and buildings) with a precision of ± 3 m. The altitude is needed to process the radiometric data. A barometric altimeter is used to determine the altitude of the helicopter above mean sea level, but this altimeter is employed only as a backup for the GPS receivers. Without a base station as reference the GPS measurements may have an error of some metres.

The altitude of the bird above the ground must be accurately known for the processing of the electromagnetic data and to generate a digital terrain model. A laser altimeter (**Table 8**) inside the bird provides this altitude with a precision of ± 0.2 m. A further advantage of the laser altimeter, in addition to its precision, is the focused laser beam allowing, compared to the radar altimeter, mostly better measurements of the true distance to the surface as it is less affected by the tree canopy.

Table 8: *Altimeters*

Altimeters		
Helicopter	Radar Altimeter	
	Function	Recording of the altitude of the helicopter above ground level
	Manufacturer	Sperry, USA
	Type	AA-200
	Barometric Altimeter	
	Function	Recording of the altitude of the helicopter above mean sea level
	Manufacturer	Rosemount, USA
Bird	Type	1241A5B
	Laser Altimeter	
	Function	Precise recording of the altitude of the HEM bird above ground
	Manufacturer	Riegl, Austria
	Type	LD90-3800VHS

The digital elevation model is derived from the GPS elevation of the HEM bird in m asl minus the laser altitude or, alternatively, from the GPS elevation of the helicopter in m asl minus the radar altitude. Without a base station as reference for the GPS measurements, and thus, the topographic elevations may have an error of some metres.

4.7. Data Acquisition and Recording

The HeliDas system stores all the data digitally on CF card during a survey flight (**Table 9**). The data sets are ready for processing with GEOSOFT OASIS montaj. The most important data channels are also displayed on the tablet computers to enable continual checking of the data during the flight. Immediately after a flight, the digital data are copied to a field computer and checked more accurately in order to obtain an impression of the geophysical results and to detect any problems with the survey system.

Table 9: *Data acquisition and recording systems*

Data acquisition and recording systems		
Helicopter	Function	Digitisation of the analogue signals, buffering of all digital data; flight path and displaying of selected data channels; storage of position and field data on CF card ready for processing with GEOSOFT OASIS montaj
	Manufacturer	FAS, Canada
	Type	HeliDas

4.8. Video System

A video camera (**Table 10**) is mounted in the bottom of the helicopter. Two monitors, one in the cockpit and one in the operator's rack, allow monitoring of the bird at take-off and landing as well as during the flight.

The video recording of the flight path is used to locate sources of anomalous or disturbed data on the ground. The flight path video can be correlated directly with the digital data.

Table 10: *Video system*

Video system		
Helicopter	Function	Recording of the flight track and monitoring of the movements of the HEM bird during take-off, landing and flight
	Manufacturer	Colour camera: Sony, Japan Video recorder: AXI, Sweden
	Type	Colour camera: DC372P Video server: AXIS 241S

4.9. Additional Equipment

The 28 V DC on-board voltage of the helicopter is smoothly buffered by a 24 Ah battery and connected to a central power unit. From there it is distributed to the individual components of the system with built-in fuses to protect devices from overvoltage (**Table 11**).

Control and recording units of the airborne geophysical system are mounted in a 19" rack. Shock absorbers between the base of the rack and a wood board which is firmly screwed to the floor of the helicopter minimize the transfer of vibrations originating from the rotor (**Table 11**).

Table 11: *Additional equipment*

Additional equipment		
Helicopter	Central power unit	
	Function	28 V DC on-board voltage of the helicopter buffered by a 24 Ah buffer battery and connected to a central power unit
	Manufacturer	Sikorsky, USA
	Instrument rack	
	Function	19" rack on shock absorbers to mount all components of the airborne geophysical system
	Manufacturer	Sikorsky, USA

5. Processing and Presentation of the Survey Data

The general objectives of the data processing may be summarized as follows:

- quality control of the measured data;
- conversion of the field data into physical parameters;
- presentation of the results as maps and vertical sections.

5.1. General Processing Steps

The airborne geophysical data are copied from the CF card to field computers directly after a survey flight in order to save the data and to check them for plausibility and correctness. Using the software GEOSOFT OASIS montaj, the primary field data processing steps are conducted automatically, followed by a pre-processing of all survey data in order to display preliminary results.

The final data processing starts with the processing of the position data:

- coordinate transformation;
- correction of altitude data of the helicopter and the bird.

The following processing steps are valid for all methods:

- removal of spiky data;
- reduction of high-frequency noise by digital filtering;
- conversion of the data to the desired geophysical parameters;
- fixing of the ends of the profiles for splitting the flights into profiles;
- merging the flight-line data sets to area data sets;
- levelling of the data;
- storage of the final survey data and geophysical parameters;
- production of maps and vertical sections (only HEM).

The field data processing and the calculation of the physical parameters for each method are described in more detail in the following chapters. GEOSOFT OASIS montaj is used throughout if not otherwise noted.

5.2. Position Data

5.2.1. Coordinates

The coordinates of the helicopter and the bird recorded during the survey flight refer to the WGS 84 geographic coordinate system. These geographic coordinates are transformed to local Cartesian coordinates. False coordinates are corrected and gaps are interpolated.

All survey results refer to UTM WGS 84 coordinates (3° meridian, zone 31N).

5.2.2. Elevation

The accuracy of the GPS elevation of the helicopter and the bird is generally not sufficient without post-processing. The application CSRS, a service provided by the Natural Resources Canada (http://www.geod.nrcan.gc.ca/online_data_e.php), enables a reduction of the position error of less than 0.3 m for all components. Required is a full GPS data set converted to the RINEX format. Currently only the GPS data of the helicopter can be corrected this way. Thus, the accuracy of GPS data of the bird is generally not very accurate.

5.2.3. Radar Altitude

The radar altitude data measured in feet at the helicopter ($h_{r_{mess}}$) are transformed to metres above ground level (m agl)

$$h_{r_heli} [m] = h_{r_{mess}} [ft] \cdot 0.3048 [m/ft] \cdot r_c,$$

where

h_{r_heli}	=	adjusted radar altitude of the helicopter (unit: m agl),
$h_{r_{mess}}$	=	radar altitude (unit: ft) measured by the altimeter,
r_c	=	correction factor (1.03).

As the radar beam is not directed exactly vertical, a correction is necessary. The correction factor (r_c) is derived from the ratio of the GPS elevation of the helicopter and the elevation derived from the DEM (see **Section 5.2.5**) and the radar altitude.

For the purpose of replacement of missing laser altitude data of the bird (h_l), the radar altitudes are also referred to the bird altitude (h_r)

$$h_r [m] = h_{r_heli} [m] - c_l [m],$$

where c_l is the effective cable length (offset) derived from the differences of the GPS elevations of the helicopter and the bird (about 42.5 m on average).

5.2.4. Laser Altitude

As no laser altitude data were available due to connection problems, the laser altitude was estimated as the difference of the GPS elevation of the bird and the DEM (see **Section 5.2.5**). Unfortunately, DEM data were not available off-shore and the GPS elevation of the bird was not sufficiently accurate to derive estimated laser altitudes having the accuracy of laser altimeter measurements. Drifts and offsets occurred causing bird altitude errors of up to several metres.

In order to get better bird altitude data, the topographic relief derived from the HEM inversion (see **Section 5.3.7**) was used to estimate corrections for all altitude data. The offsets were derived from the smoothed differences of the inverted model surface elevation and (off-shore) measured topographic relief or (on-shore) the DEM.

5.2.5. Topographic Elevation

The topographic relief (topo) is generally derived from the difference of the GPS elevation of the bird (h_{GPS}) and the corrected laser altitude (h_{lkor}). As no laser altitude data were available in this survey, the topographic relief was derived from the difference of the GPS elevation of the helicopter ($h_{\text{GPS_heli}}$) and the radar altitude of the helicopter ($h_{\text{r_heli}}$)

$$\text{topo [m asl]} = h_{\text{GPS_heli [m asl]}} - h_{\text{r_heli [m]}}.$$

The accuracy of this topographic relief was often not sufficient for the elevation setting of the HEM models (see **Section 5.3.8**) due to helicopter measurements affected by GPS and helicopter attitude errors. Thus, on-shore the digital elevation model (DEM, derived from laser altimetry (AHN1) and provided by the Dutch project partners) was used.

5.3. Processing of the Electromagnetic Data

The evaluation of the measured I and Q values (in ppm), i. e., the real part (in-phase or 0°-phase) and the imaginary part (out-of-phase, quadrature or 90°-phase) of the relative secondary field requires several processing steps:

- application of calibration factors;
- zero-level and drift correction;
- data correction;
- transformation to half-space parameters;
- correction of man-made effects;
- levelling;
- interpolation and smoothing;
- inversion to resistivity models.

While the half-space parameters, apparent resistivity and the centroid depth, are individually derived from secondary field values for each frequency, the final resistivity models are calculated at each survey point by 1-D inversion of the data of all (or selected) frequencies.

5.3.1. Calibration of the HEM System

The HEM system was calibrated by the manufacturer (FAS) on highly resistive ground in Mounts-burg Conservation Area, Canada. After adjusting the phase with the help of a ferrite rod, well-defined external calibration coils were used to derive the ppm values of the internal calibration coils. These calibration factors are used to convert the voltages measured during a survey flight to ppm values representing the secondary magnetic fields (**Table 12**).

Table 12: Calibration factors of the HEM system

Frequency [Hz]	Calibration factors FAS		Calibration factors BGR	
	I [ppm]	Q [ppm]	I [ppm]	Q [ppm]
387	-205.3	-205.3	-209.8	-210.8
1,821	-175.4	-174.7	-174.7	-174.3
5,407	76.6	76.8	81.9	81.2
8,395	-144.4	-144.2	-209.4	-198.8
41,440	-667.3	-665.2	-657.4	-664.9
133,300	-1404.2	-1406.4	-685.5	-911.0

At the beginning of each survey flight and at high flight altitude, phase and gain of the EM system are adjusted automatically for each frequency using internal calibration coils. Due to instrumental drift, the calibration has to be checked several times during the flight. The calibration signals caused

by internal calibration coils are compared with known calibration signals and phase shifts and gain correction factors are applied to the data.

As a mutual coupling with the subsurface during the ground calibration procedure and technical changes of the system caused modified calibration factors, a flight over highly conductive North Sea water in February 2009 was used to check the calibration values. The evaluation of this data set yielded a set of phase and gain corrections being enormous particularly for the 8.3 and 133 kHz frequency data (**Table 13**).

A further check of the calibration factors based on over-water flying (Westerschelde) yielded an updated set of mean phase and gain errors which were applied to the data during data processing. Except the corrections for the highest frequency ($f = 133$ kHz: gain error 17% and phase shift 10° to 15°), the corrections necessary were generally small ($\leq 2\%$ gain and $\leq 0.5^\circ$ phase). A final check of the preliminary inversion models (see **Section 5.3.7**) yielded an unrealistic thin conductor throughout and another set of phase and gain errors were obtained by suppressing the conductor (normally $\leq 1\%$ gain and $\leq 0.5^\circ$ phase, but for 8.3 kHz 6% gain and for 387 Hz 5% gain). Thus, gain corrections of 1.06 and 0.95 were applied to the data of the 8.3 kHz and 387 Hz frequencies during inversion, respectively.

5.3.2. Zero-Level and Drift Correction

The signals measured by the receivers may still contain some non-compensated parts of the primary fields generated by the transmitters. These so called zero levels may also have thermal drift. The zero levels of the HEM data are generally determined at high flight altitudes (>350 m) several times during a survey flight as the ground response is negligible at this altitude, i. e., the secondary field should be close to zero. Zero-level reference points are set at such high-altitude profile segments, preferably where the signal is not noisy. The zero level is obtained individually for each data channel by linear interpolation of the picked values at adjacent zero level reference points.

This procedure enables to remove the long-term, quasi-linear drift. Short-term variations, however, caused by temperature changes due to altitude variations, which occur particularly in the highest-frequency data, cannot be corrected successfully by this procedure. Therefore, additional reference points – also along the profiles at normal survey flight altitude – have to be determined where the secondary fields are small but not negligible. At these locations, the estimated half-space parameters are used to calculate the expected secondary field values, which then serve as local reference levels (Siemon, 2009). As this drift correction procedure is often not sufficient, statistical levelling procedures have to be applied in addition (see **Section 5.3.6**).

5.3.3. Data Correction

Noise from external sources (e. g., from radio transmitters, power lines, sferics, built-up areas, streets, railway tracks) is eliminated from the HEM data by appropriate filtering or interpolation. All those field values (I or Q) are automatically eliminated which fall below the relative standard error (rel. STE = $STE/Mean$) of the field values within a given data window. The field values are smoothed using a combination of non-linear (Naudy & Dreyer, 1968) and low-pass filters to exclude outliers

and to suppress high-frequency noise, respectively. Due to frequency dependent data qualities the data channels are treated individually (**Table 13**).

Induction effects from buildings and other electrical installations (see **Section 5.3.5**) or effects from strongly magnetized underground sources are normally not erased from the data during the initial stage of data processing.

Table 13: Filter parameters for HEM data processing

Frequency [Hz]	Mean / STE [Values]	Threshold of rel. STE	NL filter Values/Tolerance	LP filter T _{LP} [Values]
387	75 / 25	0.05	20 / 3.0	40
1,821	75 / 25	0.05	20 / 2.0	30
5,407	75 / 20	0.05	10 / 2.0	30
8,395	75 / 15	0.05	10 / 2.0	30
41,440	75 / 15	0.05	5 / 2.0	30
133,300	75 / 15	0.05	5 / 2.0	30–50

5.3.4. Conversion of the Secondary Field Values to Half-Space Parameters

The relative secondary magnetic field $Z = (I_c, Q_c)$ for a horizontal-coplanar (HCP) coil pair with a coil separation r is calculated at an altitude h above the surface and at a frequency f by (e. g., Ward & Hohmann, 1988)

$$Z = r^3 \int_0^{\infty} R_1(f, \lambda, \rho, \mu, \epsilon) \frac{\lambda^3 e^{-2\alpha_0 h}}{\alpha_0} J_0(\lambda r) d\lambda$$

where $\alpha_0^2 = \lambda^2 - \omega^2 \mu_0 \epsilon_0 + i\omega \mu_0 / \rho_0$ with $\mu_0 = 4\pi \cdot 10^{-7}$ Vs/Am, $\epsilon_0 = 8.854 \cdot 10^{-12}$ As/Vm and $\rho_0 > 10^8 \Omega m$, J_0 is a Bessel function of first kind and zero order, and R_1 is the complex reflection factor containing the material parameters (electric resistivity ρ , magnetic permeability μ and dielectric permittivity ϵ) of the subsurface. This complex integral is evaluated numerically using fast Hankel transforms (e. g., Anderson, 1989, Johansen & Sørensen, 1979). A similar formula exists for a coaxial coil (VCX) configuration yielding smaller ppm values (VCX $\approx -0.25 \cdot$ HCP). Following Weidelt (1991) the reflection factor R_1 for a N-layer half-space model is derived by a recurrence formula

$$R_1 = \frac{B_1 - \alpha_0 \mu / \mu_0}{B_1 + \alpha_0 \mu / \mu_0}$$

with

$$B_n = \alpha_n \frac{B_{n+1} + \alpha_n \tanh(\alpha_n t_n)}{\alpha_n + B_{n+1} \tanh(\alpha_n t_n)} \quad n=1,2,\dots,N-1 \quad \text{and} \quad B_N = \alpha_N$$

$$\alpha_n = \sqrt{\lambda^2 - \omega^2 \epsilon_n \mu_n + i\omega \mu_n / \rho_n} \quad n=1,2,\dots,N$$

where ρ_n , μ_n , ϵ_n and t_n are resistivity, permeability, permittivity and thickness of the n^{th} layer, respectively (t_N is assumed to be infinite). As magnetic effects and displacement currents are negligible, i. e., $\mu_n = \mu_0$, and $\epsilon_n = \epsilon_0$ only resistivities and depths are taken into account (**Fig. 4**).

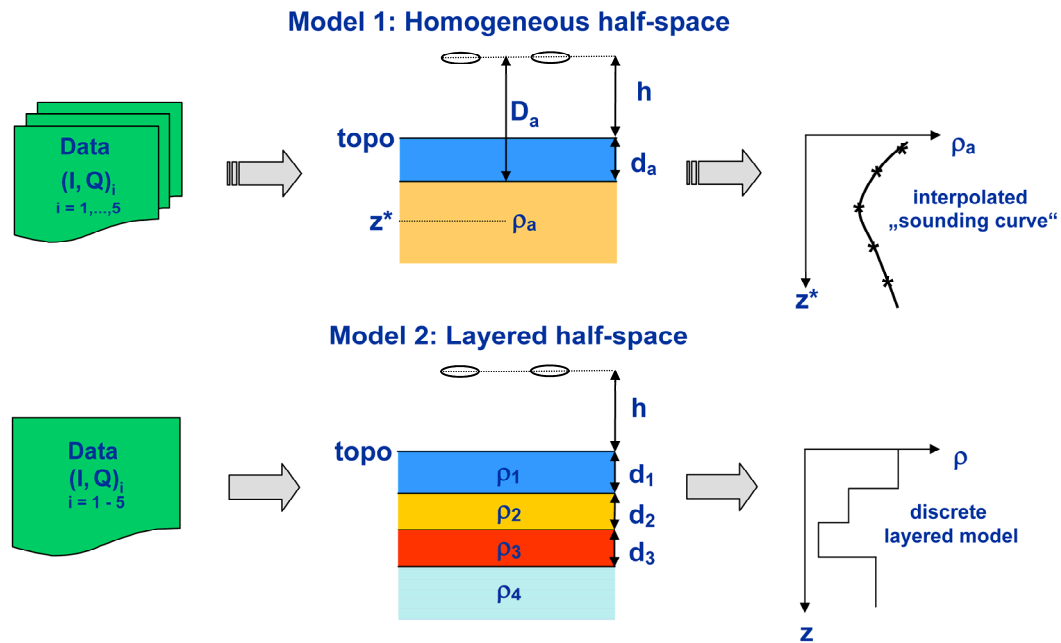


Fig. 4: HEM inversion based on a homogeneous half-space or a layered half-space

Calculated secondary field values I_c and Q_c (in ppm) are used to convert the calibrated measured values (I and Q) to the parameters of a homogeneous half-space (Siemon, 2001),

- apparent resistivity ρ_a [Ωm] and
- apparent distance D_a [m] from the sensor to the top of the conducting half-space,

individually for each frequency.

For this, the reduced amplitude $A'_c = (h/r)^3 \cdot A_c$ with $A_c = (I_c^2 + Q_c^2)^{1/2}$ and the ratio $\epsilon_c = Q_c/I_c$ are calculated for an arbitrary half-space as a function of the ratio $\delta = h/p$ of sensor altitude h and skin depth $p = 503.3 \cdot (\rho_a/f)^{1/2}$.

The half-space parameters are then derived for each pair of measured secondary field values from the functions $A'_c(\delta)$ and $\delta(\epsilon_c)$ approximated by polynomials ($A'_p(\delta)$ and $\delta_p(\epsilon)$):

$$D_a = r (A'_p(\delta_p(\epsilon))/A)^{1/3} \quad \text{and} \quad \rho_a = 0.4 \pi^2 f (D_a/\delta_p(\epsilon))^2.$$

The calculated distance D_a may differ from the observed HEM sensor altitude (in m above ground level), i. e., the top of the conducting half-space model needs not to coincide with the surface of the earth as determined by the altimeter. The difference between the two quantities is defined as the apparent depth $d_a = D_a - h$. If d_a is positive, a resistive cover is assumed above the half-space. If d_a is negative, a conductive cover is assumed.

In addition to the apparent resistivity ρ_a and apparent distance D_a , the centroid depth $z^* = d_a + p/2$ is determined (Siemon, 2001). The centroid depth is a measure of the mean penetration of the induced

underground currents. The resulting sounding curves $\rho_a(z^*)$ provide a initial approximation of the vertical resistivity distribution.

The actual approach for calculating the half-space parameters differs from that described by Siemon (2001) as the field values are calculated more accurately, particularly at higher frequencies, and the polynomial approximation of the functions $A'(\delta)$ und $\delta(\epsilon)$ are optimised for each individual frequency.

The half-space parameters are checked for plausibility, i. e., high altitude ($h > 100$ m) and extreme ($\rho_a > 1000 \Omega\text{m}$, $d_a > 100$ m) values have been eliminated before they are used for further processing.

5.3.5. Effect of Anthropogenic Influences on the HEM Data

In addition to the geogenic contribution to the secondary fields measured over densely populated areas, there is often an anthropogenic contribution from buildings and electrical installations etc. Generally, these have little influence on the HEM data and the data can be corrected using the standard data processing tools. In some cases, e. g., large buildings with a high metal content, the anthropogenic components in the HEM data are no longer negligible. Furthermore, external electromagnetic fields exist close to power lines, electric railway tracks or built-up areas which are able to substantially affect the HEM measurements. These man-made effects appear particularly in the lower frequency data because the geogenic contribution to the secondary fields is comparatively smaller at lower than at higher frequencies and, thus, the anthropogenic contribution, which is rather frequency independent, may dominate.

The anthropogenic influence lowers the calculated resistivity and associated depth. Thus, low resistivity and depth pattern on maps and sections often correlate with man-made effects such as villages or streets. These man-made effects can be detected in the HEM data due to their typical shape or by correlation with magnetic data. Topographic or Google Earth maps of the survey area, an analysis of the video records or an on-site inspection can help identify such effects.

A manual correction of man-made effects is very time consuming as each HEM channel of each survey line has to be examined individually. Therefore, a semi-automatic filter procedure has been developed and integrated into GEOSOFT OASIS montaj software. This procedure uses the gridded data of the half-space parameters apparent resistivity and apparent depth. These grids are inspected (once or several times) for anomalous data. Minimum and/or maximum anomalies are detected when the differences of the grid values and their corresponding median values, which are calculated in circular areas shifted over the grid, exceed a given threshold (**Table 14**).

A topographic map and a Google Earth map are used to check whether the corresponding data segments are affected due to man-made sources and – if necessary – the data are reinstalled in manually selected areas. In order to close the remaining data gaps one can either apply gridding and resampling tools on the grids or use a spline interpolation along each survey line. Afterwards the HEM data are recalculated from the corrected half-space parameters. The measured HEM data are replaced by the calculated HEM data where the semi-automatic procedure has cut the data out.

Table 14: Filter parameters for semi-automatic identification of man-made effects

Frequency [Hz]	Radius [m] $\log \rho_a / d_a$	Threshold $\log \rho_a / d_a$	Number of passes $\log \rho_a / d_a$	Type of anomaly $\log \rho_a / d_a$
387	5 / 5	0.30 / 3.7	1 / 1	Min. / Min.
1,821	5 / 5	0.18 / 2.7	1 / 1	Min. / Min.
5,407	5 / 5	0.20 / 3.0	1 / 1	Min. / Min.
8,395	5 / 5	0.17 / 2.7	1 / 1	Min. / Min.
41,440	5 / 5	0.19 / 3.0	1 / 1	Min. / Min.
133,300	5 / 5	0.37 / 3.7	1 / 1	Min. / Min.

5.3.6. Statistical Levelling

In order to identify and to correct zero-level errors in the HEM data a grid based micro-levelling is applied to the half-space parameters ($\log \rho_a$ and d_a) of the parallel survey lines. The procedure uses a combination of two filters: Butterworth (high pass, cut-off value: 500 m, degree: 10) and directional cosine (pass, azimuth: 0°, degree: 1). The resulting error grids are resampled along the survey lines and smoothed using a B-Spline filter (smoothness: 1.0, tension: 0.5). These smoothed error channels are then subtracted from the half-space parameters.

Strong HEM anomalies are normally smoothed by the two-dimensional lateral filtering of the micro-levelling procedure. Therefore, grids where the local anomalies have been removed beforehand are used for micro-levelling. This results in rather smooth apparent resistivity and apparent depth maps.

The tie lines are levelled afterwards using the levelled line grids as reference. The smoothed (B-Spline, smoothness: 1.0, tension: 0.5) differences of levelled and unlevelled half-space parameters are used to correct the tie-line data.

The levelled half-space parameter values are then converted to secondary field values (I_c , Q_c) which are compared with the corresponding unlevelled and not filtered values. Selected parts of the differences of the levelled and unlevelled values ($\Delta I = I - I_c$, $\Delta Q = Q - Q_c$) are strongly smoothed using a non-linear filter and a smoothing spline interpolation. The selection is based on constant (data noise, system altitude) and dynamic (I_{spline} , Q_{spline}) threshold values (**Table 15**). These interpolated smoothed differences are assumed to characterize the zero-level errors and they are used to correct the HEM data without losing details (Siemon, 2009).

Table 15: Filter parameters for the levelling of HEM data

Type of filter	Filter parameters	Channel
Threshold	Cut-off value (h_{1kor}): 300 m	$\Delta I, \Delta Q$
Threshold	Cut-off value (I_{noise}, Q_{noise}): 0.05	$\Delta I, \Delta Q$
B-Spline	Smoothness: 1.0, tension: 0.2	I, Q
Non linear	Window length: 50 points (≈ 200 m), tolerance: 3.0	$\Delta I, \Delta Q$
B-Spline	Smoothness: 0.95, tension: 0.5	$\Delta I, \Delta Q$

Finally, the levelled data values are processed following the procedure described in **Section 5.3.3** with changed filter parameters (**Table 16**). Noisy data are replaced by model data (I_c, Q_c) if the bird altitude is higher than 100 m or the relative standard error referred to the model data exceeds a given threshold.

Table 16: Filter parameters for levelled HEM data

Frequency [Hz]	STE [Values]	Threshold of rel. STE	NL filter Values/Tolerance	LP filter T_{LP} [Values]
387	100	0.03	15 / 3.0	40
1,821	100	0.03	15 / 3.0	30
5,407	100	0.03	15 / 3.0	30
8,395	100	0.03	15 / 3.0	30
41,440	100	0.03	15 / 3.0	30
133,300	100	0.03	15 / 3.0	30

The levelling is done prior to the 1-D inversion of the HEM data.

5.3.7. 1-D Inversion of the HEM Data

The model parameters of the 1-D inversion are the resistivities ρ and thicknesses t of a layered half-space (Fig. 4), where the thickness of the underlying half-space is assumed to be infinite. Marquardt's inversion procedure is used (Sengpiel & Siemon, 2000), which requires a starting model. This starting model is derived from the apparent resistivity vs. centroid depth values $(\rho_a, z^*)_i$, $i = 1, \dots, n$ (Fig. 5).

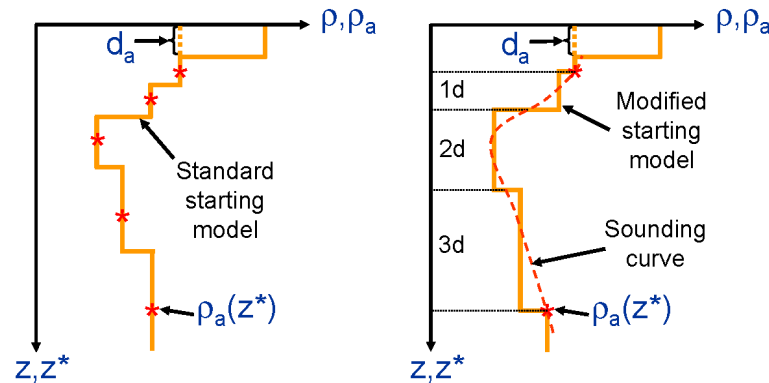


Fig. 5: Construction of starting models derived from apparent resistivity ρ_a , centroid depth z^* and apparent depth d_a of a five-frequency HEM data set

The standard starting model (Siemon, 2006) is constructed with respect to the number of frequencies used, i. e., the number of layers is given and the model layers correspond to the apparent resistivities and centroid depths of each frequency. The layer resistivities are set equal to the apparent resistivities, the layer boundaries are chosen as the logarithmic mean of each two neighbouring centroid depth values. The use of the standard starting model enables the highest resolution, but also the highest sensitivity to calibration errors. Therefore, a modified starting model is constructed having an arbitrary number of layers. The resistivities and depths of the first and last layers are derived from the apparent resistivities and centroid depths of the highest and lowest frequencies, respectively. These confining layer boundaries can be shifted upwards or downwards. The thicknesses of the intermediate layers increase linearly and the resistivities are picked from an apparent resistivity sounding curve at the corresponding layer centres (on a log scale). Optionally, a resistive cover layer may be used. The thickness of the cover layer is derived from the apparent depth d_a of the highest frequency. If this apparent depth value is less than a minimum layer thickness value, the latter value (e. g., 0.5 m) is used.

The inversion procedure is stopped when a given threshold is reached. This threshold is defined as the differential fit of the modelled data to the measured HEM data. Normally a 10% threshold is used; i. e., the inversion stops when the enhancement of the fit is less than 10%.

The data of 5.5 kHz frequency were not used for inversion as they are obtained with a vertical coaxial coil system being sensitive to steeply dipping conductors (and also to external sources) whereas all others are obtained with horizontal coplanar systems.

The survey data were inverted with starting models having five and fifteen layers. For the latter, the smooth inversion, fixed layer thicknesses were used. Only the cover-layer thickness was allowed to vary.

5.3.8. Presentation of the Results

The HEM results are presented on maps and vertical resistivity sections (VRS). The maps are produced for the half-space parameters, apparent resistivity and centroid depth, as well as for resistivities at eight depth levels (1–20 m below sea level) picked from fifteen-layer inversion models. In addition to that a map which displays the depth to the salt water (D_s) is derived from the inversion models by accumulating the top layer thicknesses where the corresponding layer resistivities exceed $7 \Omega\text{m}$. All the maps prepared from the results of this survey are listed in **Section 6.3**.

All data points used for the production of apparent resistivity and centroid depth maps are drawn as small black dots (flight lines). White dots mark areas of interpolated data. On the maps displaying resistivities at certain elevations or the depth to the salt water, the white dots inform about the number (frequencies) of interpolated data sets: the bigger the dot the more interpolated data were used for the inversion.

The VRS, also based on the 1-D inversion results, are produced for each of the survey lines. These vertical sections are constructed by placing the resistivity models for each sounding point along a survey profile next to each other using the topographic relief as base line (in m asl). The thickness of the bottom layer (substratum) is derived from the corresponding resistivity, but the minimum thickness is 5 m. The altitude of the EM sensor, information about the data processing, the fitting error of the inversion, and the HEM data, which are described in a legend, are plotted above the resistivity models.

5.4. Processing of Magnetic Data

5.4.1. Magnetic Total Field

The earth's total magnetic field T at a point r and at a time t , e. g., measured with an airborne system, is the sum of the following parts:

$$T(r,t) = F(r) + \Delta V(t) + \Delta T(r) + \delta_T(r,t),$$

where

- $F(r)$ = geomagnetic main field (IGRF = International Geomagnetic Reference Field),
- $\Delta V(t)$ = diurnal variations of the earth's magnetic field,
- $\Delta T(r)$ = the crustal field in the survey area,
- $\delta_T(r,t)$ = anthropogenic part of the magnetic field.

The anomalies of the crustal field $\Delta T(r)$ caused by rock magnetization are of interest. While the IGRF $F(r)$, which can be calculated from table values, and the diurnal variations $\Delta V(t)$, which are recorded at the base station, can be subtracted from the measured total field, the anthropogenic part $\delta_T(r,t)$ cannot be quantified independently. Therefore, the derived ΔT values contain both the geogenic part and the disturbing anthropogenic part. Anthropogenic sources are located at the earth's surface (e. g., buildings, power lines, industrial sites). They are mostly locally constrained and thus can be identified using maps and other sources of information.

5.4.2. IGRF

The IGRF (International Geomagnetic Reference Field) can be calculated for any point on and above the earth's surface at a specific time on the basis of spherical harmonic coefficients, which are updated every five years by the International Association of Geomagnetism and Aeronomy (IAGA, 1992). The geomagnetic main field values of the survey area were calculated for each point using the IGRF-10 model from 2005 (IAGA, 2005).

5.4.3. Diurnal Variations

The base station for recording the time variant parts of the total magnetic field, the diurnal variations, was placed on the airport Midden Zeeland at 3°43'20"E, 51°30'48"N and 2 m asl. Due to a malfunctioning the data recorded by the station were erroneous. Therefore, magnetic recordings of the German geomagnetic observatory Niemegk, located at 12°40'30"E, 52°04'20"N, were used for the processing of the magnetic data. $\Delta V(t)$ values are calculated as the value measured at the observatory minus the IGRF value for the respective time and place. Possible disturbances are eliminated using despiking and low-pass (filter width: 20) filters.

5.4.4. Levelling

After subtraction of the main field and diurnal variations from the measured magnetic field values, a statistical levelling is performed. The differences at the intersections of the flight lines and the tie lines are determined and averaged for each flight. The averaged values are then used to correct level errors that may occur in case of changes in the setup of the airborne or base station magnetic sensors during the survey.

Remaining, mostly small level errors may occur, inter alia, as result of different flight directions (heading errors) and are eliminated in a subsequent micro-levelling process. Micro-levelling is based on gridded line data in which level errors are identified using two-dimensional Butterworth high-pass (cut-off value: 1600 m, degree: 4) and directional cosine FFT (azimuth: 8°, degree: 1) filters. Result of the filtering process is an error grid which is sampled along the flight lines. The sampled error values are heavily smoothed using a B-Spline filter (smoothness: 1.05, tension: 0.5) and then subtracted from the original data. Gridding of the levelled data yields a ΔT grid that is virtually free of level errors. Finally, the tie-line data are fit to the levelled line-data grid by removing possible offsets and trends in their differences.

In (partly) populated areas, grids of ΔT values are mostly dominated by high-amplitude anthropogenic anomalies. These anomalies act as a source of disturbance during the micro-levelling process as well as during the identification of weak geogenic magnetic anomalies. Therefore, a semi-automatic filter procedure is applied to the data prior to micro-levelling. The procedure detects anomalous data in the ΔT grid. Anomalies are detected when the differences of the grid values and their corresponding median values, which are calculated in circular areas shifted over the grid, exceed a given threshold. Manual interaction in the detection process is possible. The resulting grid is, as far as possible, freed from anthropogenic anomalies and is used as input for the micro-levelling process. The anthropogenic regions blanked in the finally levelled data are re-introduced by applying error values interpolated from neighbouring data sections to them. The levelled data are used to produce a final ΔT grid based on all data including anthropogenic anomalies.

5.4.5. Presentation of the Results

The maps produced to display the magnetic anomaly data are listed in **Section 6.3**. All data points used for map production are drawn as small black dots (flight lines).

5.5. Processing of Gamma-Ray Spectrometry Data

The natural gamma radiation of rocks and soil is mainly generated by the radioelements potassium, uranium, and thorium. According to the recommendations of the IAEA (2003), the spectrometry data recorded in the aircraft have to be converted to equivalent ground concentrations of these elements. This requires some preparatory procedures regarding spectrometer calibration and a number of data processing steps listed below.

Spectrometer calibration:

- Determination of cosmic and aircraft background count rates by means of flights over extensive water bodies
- Determination of stripping ratios for Compton scattering correction using calibration pads
- Determination of height attenuation and sensitivity coefficients by means of flights over a calibration range

Data processing:

- Energy calibration
- Reduction of count rate statistical noise
- Determination of detector height above ground and effective height
- Live time correction
- Background correction
- Compton (stripping) correction
- Height-attenuation reduction
- Calculation of equivalent ground concentrations

5.5.1. Energy Calibration

The spectral stability of gamma spectrometers is not perfect. Due to temperature effects, the mapping of energy peaks to correct channel positions may drift slightly during a survey flight. Therefore, an energy calibration is applied to the recorded spectra during data post processing. The channel-energy mapping of a spectrometer can be expressed as follows:

$$ch = E / G + offs,$$

where

ch = channel number,

E = energy in keV,

G = gain constant of spectrometer in keV/channel,

offs = channel offset.

A 256-channel spectrometer has a nominal gain constant of 12.0 keV/channel and an offset of 0 channels. In order to determine the actual gain and offset of the spectrometer used, mean spectra are calculated for each flight line. The positions of the known energy peaks in the mean spectra (K, U, Th) can then be used to calculate actual gain and offset of the instrument during each of the analysed time windows (flight lines). Based on these values, the recorded spectra are re-mapped to a nominal 12 keV/channel raster.

5.5.2. Reduction of Statistical Noise

Due to a relatively large distance between the sources of radiation at the earth's surface and the radiation detector in the helicopter, count rates in airborne gamma-ray surveys are generally low. This results in a high portion of statistical noise present in the recorded spectra and, consequentially, also present in the calculated ground concentrations of radioelements. Therefore, a method for noise reduction developed by Hovgaard & Grasty (1997) is applied to the data. The NASVD method (noise adjusted singular value decomposition) is based on a statistical analysis of all spectra recorded in a survey area and a reconstruction of noise reduced spectra using singular value decomposition routines. The procedure results in smoothed spectra reconstructed from five principal components, from which the count rates for the energy windows of interest (see **Table 6**) are determined. Furthermore, an adaptive filter (Mathis, 1987) for smoothing the count rate channels (filter width: 10) is applied.

5.5.3. Detector Height above Ground and Effective Height

Knowledge of the distance between the source of radiation (on the ground) and the detector (in the helicopter) is crucial for inferring ground concentrations of radioelements from airborne radiometric data correctly. The helicopter system used by BGR is equipped with two altimeters: a radar altimeter in the helicopter and a laser altimeter in the EM bird. The radar altimeter data are used to determine the detector's height above ground because it is installed on the same platform.

In order to apply the radiometric analysis techniques, it is necessary to convert actual environmental conditions of the survey to standard conditions. This includes the adjustment of the measured ground clearance to standard temperature and pressure (STP conditions). The adjusted ground clearance value called “effective height” has the same mass of STP air between the ground and the helicopter as the actual one during data acquisition. The adjustment is applied according to IAEA (2003):

$$h_e = (h_r \cdot P \cdot T_0) / (P_0 \cdot (T + T_0)),$$

where

- h_e = effective height above ground level at STP [m],
- h_r = helicopter height above ground, determined from corrected radar altimeter data [m],
- T_0 = 273.15 K; freezing point of water on Kelvin scale,
- T = air temperature [°C],
- P_0 = 101.325 kPa; mean air pressure at sea level,
- P = barometric pressure [kPa].

5.5.4. Live Time Correction

Gamma-ray spectrometers need a certain amount of time to process a pulse detected by the system. During that time, further incoming pulses are rejected. The amount of time the system is able to detect pulses (“live time”) is recorded by the system. Due to the statistical nature of gamma radiation a correction of measured count rates in order to obtain count rate values for a nominal 1 s integration interval (IAEA, 2003) is easily achieved by the following formula:

$$N = n \cdot 10^3 / t_l,$$

with

- N = corrected count rate,
- n = raw count rate,
- t_l = system live time in milliseconds.

5.5.5. Background Radiation Correction

Cosmic radiation background is caused by high-energy (>3 MeV) cosmic ray particle interaction with the atmosphere. Another source of background radiation is the immanent radioactivity of the helicopter and its equipment. Background radiation distorts the measurements of geogenic radiation and has to be corrected for. The required correction coefficients are determined by means of flights over extensive water bodies at altitudes between 100 and 3500 m. The background correction is applied according to the following formula:

$$N = a + b \cdot C,$$

where

- N = combined cosmic and aircraft background for each channel,
- a = aircraft background for each channel,
- b = cosmic rate stripping factor for each channel,
- C = low-pass filtered cosmic channel (> 3 MeV) count.

The values a and b were determined using data from test flights at different altitudes over the North Sea in 2008. For each channel K, U, Th, and TC (total count) a linear regression of the count rates for different altitude intervals and the filtered cosmic channel count rates revealed values for a and b. The values are listed in **Table 17**.

Table 17: Aircraft background and cosmic stripping factors

Channel	Aircraft background a [cps]	Cosmic stripping factor b
TC	31.09	0.722
K	5.51	0.041
U	0.48	0.033
Th	0.33	0.041

5.5.6. Compton Correction

Compton scattering leads to certain amounts of radiation from one energy window being scattered into other energy windows. For example, some amount of thorium radiation will be scattered into lower energy windows such as uranium and potassium. The removal of these effects (Compton correction) is done using so-called stripping ratios. These coefficients describe the magnitudes of scatter between the energy windows of interest. They were determined in 2008 using portable calibration pads (Grasty et al., 1991) and are listed in **Table 18**.

Table 18: *Stripping ratios*

	Stripping ratio	Value
Th → U	α	0.2485
Th → K	β	0.3852
U → K	γ	0.6599
U → Th	A	0.0395

The values of α , β , γ increase with altitude of the helicopter above ground level and have to be corrected on the base of STP equivalent altitude according to the following factors (see IAEA, 2003):

$$\begin{aligned}\alpha_e &= \alpha + 0.00049 \cdot h_e \\ \beta_e &= \beta + 0.00065 \cdot h_e \\ \gamma_e &= \gamma + 0.00069 \cdot h_e\end{aligned}$$

with

$$h_e = \text{equivalent height above ground level at STP in metres.}$$

To obtain the net count rates of the particular energy windows, the stripping ratios are applied to the data:

$$\begin{aligned}N_{\text{Th}(\text{corr})} &= (N_{\text{Th}} - aN_{\text{U}}) / (1 - a\alpha) \\ N_{\text{U}(\text{corr})} &= (N_{\text{U}} - \alpha N_{\text{Th}}) / (1 - a\alpha) \\ N_{\text{K}(\text{corr})} &= N_{\text{K}} - \beta N_{\text{Th}(\text{corr})} - \gamma N_{\text{U}(\text{corr})}\end{aligned}$$

where N_{Th} , N_{K} , N_{U} represent the background and STP corrected count rates, $N_{\text{Th}(\text{corr})}$, $N_{\text{U}(\text{corr})}$, $N_{\text{K}(\text{corr})}$ are the stripping corrected count rates, and α , β , γ , a are the STP corrected stripping ratios. No Compton correction is applied to the total count values (see IAEA, 2003).

5.5.7. Height-Attenuation Reduction

The intensity of gamma radiation measured in airborne surveys varies approximately exponentially with height. In order to estimate count rates at a nominal survey height of 80 m, the following formula is used:

$$N_s = N_m \cdot e^{-\mu(h_0 - h_e)}$$

where

- μ = window attenuation coefficient (per metre),
 N_m = observed count rate at STP effective height h_e ,
 N_s = corrected count rate for the nominal survey height h_0 .

The values (**Table 19**) were determined from data acquired at different heights over the Allentsteig (Austria) calibration range in 2003.

Table 19: *Height attenuation coefficients*

Window	Height attenuation coefficient μ (per metre at STP)
K	0.007733
U	0.008132
Th	0.005784
TC	0.006468

5.5.8. Radioelement Concentrations and Exposure Rate

IAEA (2003) recommends converting the count rates for the three radioelements into surface concentrations and exposure rates at ground level. The advantage is that the results of measurements with different instruments (e. g., with different crystal volumes) can be compared with each other. Conversion between count rates and concentrations is done using sensitivity coefficients (**Table 20**):

$$C = N_s / S,$$

with

- C = element concentration (K in %, eU in ppm, eTh in ppm),
 N_s = count rate for each window (after height attenuation and stripping),
 S = broad source sensitivity for the spectral window.

The calculated concentrations are expressed as equivalent concentrations eU and eTh (in ppm) and as concentrations of K (in %).

Table 20: *Sensitivity coefficients*

Sensitivity	
1 % K	= 28.42 cps
1 ppm eTh	= 1.96 cps
1 ppm eU	= 2.92 cps

The sensitivities (**Table 20**) were determined over the Allentsteig (Austria) calibration range. Concentrations calculated this way refer to an infinitely extended and permanently radiating plane. They may differ from the actual concentrations of the elements at ground surface, especially in areas of irregularly distributed radiation sources and under wet conditions. Furthermore, the presence of atmospheric radon may vary considerably during a survey. Radon can spoil radiometric data, in par-

ticular uranium concentrations inferred from count rates, because radon and uranium radiation is detected in the same energy window. Presently, there is no correction of the effect of radon radiation on airborne gamma-ray measurements implemented in our radiometric data processing routines. Absolute values of uranium concentrations indicated in the maps are therefore to be regarded with caution.

The ground level exposure rate is calculated as a function of the K, U, and Th concentrations after application of the vegetation correction:

$$E = 1.505 \cdot K + 0.653 \cdot eU + 0.287 \cdot eTh,$$

with

$$E = \text{ground level exposure rate } [\mu\text{R/h}]$$

using the following conversions (IAEA, 2003):

$$1 \% K = 1.505 \mu\text{R/h},$$

$$1 \text{ ppm eU} = 0.653 \mu\text{R/h},$$

$$1 \text{ ppm eTh} = 0.287 \mu\text{R/h}.$$

5.5.9. Data Levelling and Smoothing

Due to variations in soil moisture and radon abundance, some line-to-line level errors are visible in the grids of the count rate channels. These errors are removed by a statistical levelling process. The differences at the intersections of the flight lines and the tie lines are determined and averaged for each flight. The averaged values are then used to correct level errors. Remaining, mostly small level errors are eliminated in a subsequent micro-levelling process based on gridded line data in which level errors are identified using two-dimensional Butterworth high-pass (cut-off value: 600 m, degree: 8) and directional cosine FFT (azimuth: 8°, degree: 1) filters. Result of the filtering process is an error grid which is sampled along the flight lines. The sampled error values are heavily smoothed using a B-Spline filter (smoothness: 0.65, tension: 0.5) and then subtracted from the original data. Gridding of the levelled data yields grids that are virtually free of level errors. Finally, the tie-line data are fit to the levelled line-data grid. This is done by calculating the difference (error) between the values of the levelled line-data grid and the tie-line data, spline smoothing the error and subtracting it from the tie-line data.

Grids of the finally levelled data are slightly smoothed using a two-dimensional median filter of radius one grid cell (25 m).

5.5.10. Presentation of the Results

The results of the gamma-ray survey are presented as maps of the equivalent concentrations of the radioelements potassium, uranium, and thorium, total count, and the ground level exposure rate. The maps produced to display the radiometric data are listed in **Section 6.3**. All data points used for map production are drawn as small black dots (flight lines). White dots mark areas of interpolated data.

6. Cartographic Work

6.1. Topographic Map

A topographic map was produced as the base maps for all thematic maps displaying the airborne geophysical results. A scale of 1:25,000 was chosen for the survey area. An UTM coordinate grid, based on the WGS 84 ellipsoid, is included on the topographic maps. **Table 21** contains the corner coordinates of the map sheet.

Table 21: *Coordinates of the corners of the 1:25,000 Perkpolder topographic map sheets*

Map corners	Geographic coordinates (WGS 84)		UTM WGS 84 coordinates (Zone 31N)	
	Easting	Northing	Easting	Northing
SW	3°55'59"	51°20'23"	565000	5688000
NW	3°56'06"	51°25'14"	565000	5697000
NE	4°03'51"	51°25'10"	574000	5697000
SE	4°03'45"	51°20'19"	574000	5688000

The map is based on the »Topografische Kaart van Nederland 1:25,000«, © Topografische Dienst, Emmen. The following map sheets were used: 64H Goes, 67F Zaamslag, 49C Krabbendijke and 55A Hulst.

The map has a digitally constructed border and tick marks indicating coordinates in the WGS 84 coordinate system. The grey-shading of the topography of the thematic map has a screen density of 50% of the original digital topographic map.

6.2. Map Production with GEOSOFT and GIS Software

The geophysical grids for the thematic maps were produced using the software package GEOSOFT OASIS montaj 7.2. **Table 22** shows the grid parameters used for the Perkpolder survey.

Table 22: *Grid parameters*

Parameter	Value
Gridding method	Minimum curvature
Blanking distance [m]	400
Grid size [m]	50
Search radius [m]	50
Internal tension (0-1)	0
Cell extend beyond data	4
Log option	log ρ (else linear)

The final maps including geophysical, topographical and legend information are prepared using the program ESRI ArcGIS 10. A special plug-in provided by GEOSOFT for ArcGIS (available on DVD or <http://www.geosoft.com/resources/releasenotes/plugins/arcGISplugin.asp>) is necessary to import and display the GEOSOFT grids as a layer in ArcMap. Adobe Acrobat 9.4 is used for preparing the PDF documents.

6.3. Thematic Maps

Coloured geophysical thematic maps (**Table 23, Appendix IV**) were produced at a scale of 1:25,000 for each parameter of interest.

HEM: Apparent resistivities and centroid depths
at 387 Hz, 1,821 Hz, 5,407 Hz, 8,395 Hz, 41,440 Hz, and 133,300 Hz;
Resistivities at 1, 2, 4, 7, 10, 13, 16 and 20 m below sea level (bsl);
Depth to salt water;

HMG: Anomalies of the total magnetic field;

HRD: Equivalent concentrations of the radioelements potassium, uranium, and thorium,
total count rate and ground level exposure rate.

The digital topographic map was used as base map. The surveyed flight lines are plotted in black/white containing information about the quality of the data. In addition, flight-line and elevation maps were produced.

The flight-line maps show the position of the surveyed profiles on the topographic maps. The corresponding line numbers are shown at both ends of each profile. Positions of selected time marks (records) are marked with a short or long “|”e. g., every 10th or 100th record, respectively. Every 500th record is labelled with its number. The flight-line maps permit fast and easy correlation of data from profiles and vertical sections and their position in the survey area.

The on-shore digital elevation model (DEM) has been provided by TNO/Deltares. The elevation map also contains the topographic base map and the flight lines.

7. Archiving

All data sets and plots are archived at BGR section B 2.1, Geophysical Exploration – Technical Mineralogy. The data formats are described in **Appendix II**. A technical report, the vertical sections, and the thematic maps (as PDF files) are stored together with the final data (ASCII-coded in GEOSOFT-XYZ format) on a DVD (**Table 23**). A copy of this DVD is attached to this report. The content is listed in **Appendix III**. **Appendix IV** and **Appendix V** contain copies of maps and vertical resistivity sections, respectively, reduced to smaller scales fitting the A4 format of this report.

Table 23: Content of the DVD

Directory		Description of content
\Adobe Acrobat		Adobe® Acrobat Reader in diverse versions for popular system software
\Report		Technical report of the project in PDF format
\Data...	\HEM	ASCII file with all raw data (HEM136_RAW.xyz) ASCII file with all processed data (HEM136_DAT.xyz) ASCII file with all derived parameters (HEM136_APP.xyz) ASCII files with results of the 1-D inversion (HEM136_INV_L5.xyz and HEM136_INV_L15.xyz)
	\HMG	ASCII file with data of the total magnetic field, IGRF, base station data, diurnal variations etc. (HMG136.xyz)
	\HRD	ASCII file with data of the equivalent concentrations of potassium, uranium and thorium and the total count rate (HRD136.xyz)
\Maps...	\HEM	Apparent resistivity maps and centroid depth maps at a scale of 1:25,000 for the frequencies 387 Hz, 1,821 Hz, 5,407 Hz, 8,395 Hz, 41,440 Hz, 133,300 Hz in PDF format Resistivity maps at a scale of 1:25,000 at 1, 2, 4, 7, 10, 13, 16 and 20 m below sea level based on fifteen-layer inversion results in PDF format Depth to salt water map at a scale of 1:25,000 derived from fifteen-layer inversion results in PDF format
	\HMG	Magnetic anomalies maps at a scale of 1:25,000 in PDF format
	\HRD	Maps of the equivalent concentrations of the radioelements potassium, uranium, and thorium, the total count rate and the ground level exposure rate at a scale of 1:25,000 in PDF format
	\Flight lines	Flight-line maps with topography at a scale of 1:25,000 in PDF format
	\DEM	Digital elevation models at a scale of 1:25,000 in PDF format
	\ArcGIS	Map projects for ArcGIS 10 (*.mxd) incl. legends (*.bmp), Raster data 1:25,000 (GRID) and Geosoft-Plugin for ArcGIS
	\Vertical sections	Vertical resistivity section based on five-layer and fifteen-layer inversion results for each profile of the survey area at a horizontal scale of 1:25,000 and at a vertical scale of 1:1,000 in PDF format

8. References

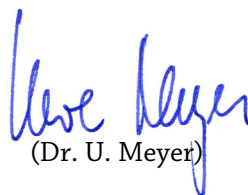
- Anderson, W.L., 1989. A hybrid fast Hankel transform algorithm for electromagnetic modelling. *Geophysics* 54, 263–266.
- Grasty, R.L., Holman, P.B. & Blanchard, Y.B., 1991. Transportable calibration pads for ground and airborne gamma-ray spectrometers. Geological survey of Canada, Paper 90-23, 25p.
- Hovgaard, J., & Grasty, R.L., 1997. Reducing statistical noise in airborne gamma ray data through spectral component analysis. In “Proceedings of Exploration 97: Fourth Decennial Conference on Mineral Exploration” edited by A.G. Gubins, 753–764.
- IAEA, 2003. Guidelines for radioelement mapping using gamma ray spectrometry data. International Atomic Energy Agency. IAEA-TECDOC-1363AEA, Vienna.
- Mathis, G.L., 1987. Smoothing spectral gamma logs: A simple but effective technique. *Geophysics*, 52, 363–367.
- IAGA, 1992. International Geomagnetic Reference Field, 1991 Revision. International Association of Geomagnetism and Aeronomy (IAGA) Division V, Working Group 8: Analysis of the main field and secular variation. *Geophys. J. Int.*, 108, 945–946.
- IAGA, 2005. International Geomagnetic Reference Field, 2005, 10th generation. International Association of Geomagnetism and Aeronomy, Division V, Working Group V-MOD. <http://www.ngdc.noaa.gov/IAGA/vmod/igrf.html>.
- Johansen, H.K. and Sørensen, K., 1979. The fast Hankel transform. *Geophysical Prospecting* 27, 876–901.
- Naudy, H. & Dreyer, H., 1968. Non-Linear Filtering Applied to Aeromagnetic Profiles. *Geophysical Prospecting*, 16, 171–178.
- Sengpiel, K.-P. & Siemon, B., 2000. Advanced inversion methods for airborne electromagnetic exploration. *Geophysics*, 65, 1983–1992.
- Siemon, B., 2001. Improved and new resistivity-depth profiles for helicopter electromagnetic data. *J. Appl. Geophys.*, 46, 65–76.
- Siemon, B., 2006. Electromagnetic methods – frequency domain: Airborne techniques. In: Kirsch, R. (ed.), *Groundwater Geophysics – A Tool for Hydrogeology*, Springer-Verlag, Berlin, Heidelberg, 155-170.
- Siemon, B., 2009. Levelling of frequency-domain helicopter-borne electromagnetic data. *Journal of Applied Geophysics*, 67, 206–218.
- Ward, S.H. & Hohmann, G.W., 1988. Electromagnetic theory for geophysical applications. In Nabighian M.N. (Eds.) *Electromagnetic methods in applied geophysics Vol. 1, Theory*. Society of Exploration Geophysics, IG no 3, Tulsa, 130–310.
- Weidelt, P., 1991, Introduction into electromagnetic sounding. Lecture manuscript. Technical University of Braunschweig, Germany.

BUNDESANSTALT FÜR GEOWISSENSCHAFTEN UND ROHSTOFFE
BGR, HANOVER



(Dr. M. Kosinowski)

Head of Department
„Groundwater and
Soil Science“



(Dr. U. Meyer)

Head of Sub-Department
„Geophysical Exploration –
Technical Mineralogy“



(Dr. B. Siemon)

Head of Unit
„Airborne Geophysics“

Appendix I

Survey Area 136 – Perkpolder

Airport:	Midden Zeeland, Elevation: 6 ft / 2 m	
Survey parameters:		
Line separation:	Lines: 200 m	Tie lines: 500 m
Line direction:	Lines: 90°	Tie lines: 0°
Line kilometre:	Lines: 129 km	Tie lines: 85 km
Size of area:	49 km ²	
Coordinate system:	WGS 84	UTM Zone 31N
Location of base station:	X: 550124 (3°43'20"E	Y: 5707165 51°30'48"N)

Table A-1: *Flight table*

Flight	Date	Time (UTC) Start – End	Lines	Remarks
13601	26.08.09	11:28 – 13:45	22.1 E 21.1 W 20.1 E 19.1 W 18.1 E 17.1 W 16.1 E 15.1 W 14.1 E 13.1 W 12.1 E 11.1 W 10.1 E 9.1 W 8.1 E 7.1 W 6.1 E 5.1 W 4.1 E 3.1 W 2.1 E 1.1 W	HELIDAS: SYS14; BKS36a (bird 61) EM: EM4 Amplitude and phase shift on all Profiles Magnetometer: ok Spectrometer: ok Video: No laser-altimeter data! Weather: sunny, 30°C, wind
13602	27.08.09	7:39 – 9:13	13.9 S 12.9 N 11.9 S 10.9 N 9.9 S 8.9 N 7.9 S 6.9 N 5.9 S 4.9 N 3.9 S 2.9 N 1.9 S 10.8 N	HELIDAS: SYS14; BKS36a (bird 61) EM: EM4 Amplitude and phase shift on all Profiles Magnetometer: ok Spectrometer: system break down on line 4.9 Video: No laser-altimeter data! Weather: cloudy, 21°C, windy

Appendix II

Final Data Format Description

A) Electromagnetics

Description of the four ASCII-coded data files containing the final (levelled) data of a helicopter-borne electromagnetic (HEM) survey

General HEADER:

/BGR HEADER (SHORT VERSION):

/

/AREANAME

/PERKPOLDER

/AREACODE

/136

/C_MERIDIAN, ZONE, REFERENCE SYSTEM

/ 3 31 WGS84

/ELLIPSOID FOR LON AND LAT

/WGS84

/BIRD

/61

/NUMFREQ

/ 6

/FREQUENCY

/ 387.00 1821.00 5407.00 8395.00 41440.00 133300.00

/COILGEOMETRY

/ 1.00 1.00 4.00 1.00 1.00 1.00

/COILSEPERATION

/ 7.94 7.93 9.06 7.93 7.91 7.92

/TOWCABLE

/ 40.00

/DUMMY

/ -999.99

/DECIMATIONVALUE

/ 1

/PRIVTEXT

(up to five lines of comment may be written here)

1) Raw data: HEM136_RAW.XYZ

Example:

/Unprocessed data

//Flight 13601

//Date 2009/08/26

Random 0

```
/ X      Y      LON_BIRD_RAW  LAT_BIRD_RAW  RECORD  UTC_TIME  ALTR  ALTL_FP  ZHG_BIRD_RAW  ZHG_HELI_RAW  ALTB  EM1I  EM1Q  ...  EM6I  EM6Q  EM1_FREQ...EM6_FREQ  CPPL  CPSP
553596  5708958  3.772639  51.529189  0  112756.0  1548.08  0.00  442.50  485.51  321.66  -40454.13 -49640.41  ... -3967.67 -1184.91  0  ...  0  0.001  0.0030
553600  5708959  3.772699  51.529197  1  112756.1  1547.93  0.00  442.58  485.61  321.04  -40454.42 -49640.23  ... -3967.75 -1184.93  4146  ...  541  0.0013  0.0013
553605  5708960  3.772758  51.529206  2  112756.2  1546.25  0.00  442.66  485.71  321.50  -40454.51 -49640.13  ... -3967.80 -1184.90  8293  ...  1081  0.0016  0.0014
```

In this data file all secondary field values are stored in the order of the following description:

Channel	Unit	Remarks
X	m	UTM easting in m (WGS 84, Zone 31N), these coordinates have a false easting of 500000 metres
Y	m	UTM northing in m (WGS 84, Zone 31N), these coordinates have no false northing
LON	°	geographic longitude, reference system WGS 84
LAT	°	geographic latitude, reference system WGS 84
RECORD		time mark increasing by 1 every 0.1 seconds
UTC_TIME	hhmmss.s	GPS time (UTC)
ALTR	ft	radar altimeter reading (helicopter)
ALTL_FP	m	laser altimeter reading (bird)
ZHG_BIRD_RAW	m	GPS elevation of the bird, reference system WGS 84
ZHG_HELI_RAW	m	GPS elevation of the helicopter, reference system WGS 84
ALTB	ft	barometric elevation of the helicopter
EM1I	ppm	raw value of the inphase component at the frequency f = 41,440 Hz
EM1Q	ppm	raw value of the quadrature component at the frequency f = 41,440 Hz
EM2I	ppm	raw value of the inphase component at the frequency f = 8,395 Hz
EM2Q	ppm	raw value of the quadrature component at the frequency f = 8,395Hz
EM3I	ppm	raw value of the inphase component at the frequency f = 387 Hz
EM3Q	ppm	raw value of the quadrature component at the frequency f = 387 Hz
EM4I	ppm	raw value of the inphase component at the frequency f = 133,300 Hz
EM4Q	ppm	raw value of the quadrature component at the frequency f = 133,300 Hz
EM5I	ppm	raw value of the inphase component at the frequency f = 1,821 Hz
EM5Q	ppm	raw value of the quadrature component at the frequency f = 1,821 Hz
EM6I	ppm	raw value of the inphase component at the frequency f = 5,407 Hz
EM6Q	ppm	raw value of the quadrature component at the frequency f = 5,407 Hz

EM1_FREQ	Hz	frequency of EM1 channels (nominally $f = 41,440$ Hz)
EM2_FREQ	Hz	frequency of EM2 channels (nominally $f = 8,395$ Hz)
EM3_FREQ	Hz	frequency of EM3 channels (nominally $f = 387$ Hz)
EM4_FREQ	Hz	frequency of EM4 channels (nominally $f = 133,300$ Hz)
EM5_FREQ	Hz	frequency of EM5 channels (nominally $f = 1,821$ Hz)
EM6_FREQ	Hz	frequency of EM6 channels (nominally $f = 5,407$ Hz)
CPPL		power-line detector
CPSP		sferics detector

Remarks:

Lines starting with "/" comment,
 Lines starting with "/" flight number and date,
 Lines starting with "Random" original flights.

Original vertical coaxial data are indicated by -1.00 (instead of 4.00 for converted data):

/COILGEOMETRY

/ 1.00 1.00 -1.00 1.00 1.00 1.00

General Remarks for the next data sets:

Lines starting with "/" comment,
 Lines starting with "/" flight number and date,
 Lines starting with "Line" lines,
 Lines starting with "Tie" tie lines.

2) Data: HEM136_DAT.XYZ

Example:

/Processing by A. Ullmann (BGR) using Oasis montaj

/GPS corrected (incl. TOPO_INV correction)

/ X Y LON LAT RECORD UTC TOPO H_RADAR H_LASER BIRD_NN H_BARO REAL_1 QUAD_1 ... REAL_6 QUAD_6

//Flight 13601

//Date 2009/08/26

Line 1.1

```
570960 5695534 4.020218 51.406585 77880 133744.0 -1.00 59.59 57.86 56.86 56.53 420.87 193.62 ... 643.33 10.94
570957 5695534 4.020176 51.406586 77881 133744.1 -1.01 58.82 57.09 56.09 55.91 433.19 201.26 ... 668.42 12.02
570954 5695534 4.020134 51.406587 77882 133744.2 -1.02 58.08 56.32 55.31 55.28 445.73 209.18 ... 695.03 13.13
```

In this data file all necessary position parameters and secondary field values are stored in the order of the following description:

Channel	Unit	Remarks
X	m	UTM easting in m (WGS 84, Zone 31N), these coordinates have a false easting of 500000 metres
Y	m	UTM northing in m (WGS 84, Zone 31N), these coordinates have no false northing
LON	°	geographic longitude, reference system WGS 84
LAT	°	geographic latitude, reference system WGS 84
RECORD		time mark increasing by 1 every 0.1 seconds
UTC_TIME	hhmmss.s	GPS time (UTC)
TOPO	m	topographic elevation (in metres above sea level)
H_RADAR	m	smoothed value of the radar altitude minus the effective cable length from the helicopter to the bird, corresponds to the bird altitude
H_LASER	m	estimated value of the laser altimeter, corresponds to the bird altitude
BIRD_NN	m	smoothed bird elevation (in metres above sea level), reference system: WGS84
H_BARO	m	smoothed value of the barometric sensor minus the effective cable length from the helicopter to the bird
REAL_1	ppm	processed value of the inphase component at the frequency f = 387 Hz
QUAD_1	ppm	processed value of the quadrature component at the frequency f = 387 Hz
REAL_2	ppm	processed value of the inphase component at the frequency f = 1,821 Hz
QUAD_2	ppm	processed value of the quadrature component at the frequency f = 1,821 Hz
REAL_3	ppm	processed value of the inphase component at the frequency f = 5,407 Hz, converted to horizontal coplanar
QUAD_3	ppm	processed value of the quadrature component at the frequency f = 5,407 Hz, converted to horizontal coplanar
REAL_4	ppm	processed value of the inphase component at the frequency f = 8,395 Hz
QUAD_4	ppm	processed value of the quadrature component at the frequency f = 8,395 Hz
REAL_5	ppm	processed value of the inphase component at the frequency f = 41,440 Hz
QUAD_5	ppm	processed value of the quadrature component at the frequency f = 41,440 Hz
REAL_6	ppm	processed value of the inphase component at the frequency f = 133,300 Hz
QUAD_6	ppm	processed value of the quadrature component at the frequency f = 133,300 Hz

3) Half-space parameters: HEM136_APP.XYZ

Example:

/Processing by A. Ullmann (BGR) using Oasis montaj

/GPS corrected (incl. TOPO_INV correction)

/ X Y LON LAT RECORD UTC TOPO H_RADAR H_LASER BIRD_NN H_BARO RHOA_1 KDA_1 ZST_1 ... RHOA_6 KDA_6 ZST_6

//Flight 13601

//Date 2009/08/26

Line 1.1

```
570960 5695534 4.020218 51.406585 77880 133744.0 -1.00 59.59 57.86 56.86 56.53 0.58 -3.98 5.75 ... 0.71 0.07 0.65
570957 5695534 4.020176 51.406586 77881 133744.1 -1.01 58.82 57.09 56.09 55.91 0.58 -3.87 5.85 ... 0.72 0.07 0.65
570954 5695534 4.020134 51.406587 77882 133744.2 -1.02 58.08 56.32 55.31 55.28 0.58 -3.75 5.97 ... 0.73 0.06 0.64
```

In this data file all necessary position parameters and half-space parameters are stored in the order of the following description:

Channel	Unit	Remarks
X	m	UTM easting in m (WGS 84, Zone 31N), these coordinates have a false easting of 500000 metres
Y	m	UTM northing in m (WGS 84, Zone 31N), these coordinates have no false northing
LON	°	geographic longitude, reference system WGS 84
LAT	°	geographic latitude, reference system WGS 84
RECORD		time mark increasing by 1 every 0.1 seconds
UTC_TIME	hhmmss.s	GPS time (UTC)
TOPO	m	topographic elevation (in metres above sea level)
H_RADAR	m	smoothed value of the radar altitude minus the effective cable length from the helicopter to the bird, corresponds to the bird altitude
H_LASER	m	estimated value of the laser altimeter, corresponds to the bird altitude
BIRD_NN	m	smoothed bird elevation (in metres above sea level), reference system: WGS84
H_BARO	m	smoothed value of the barometric sensor minus the effective cable length from the helicopter to the bird
RHOA_1	Ωm	apparent resistivity at the frequency f = 387 Hz
KDA_1	m	apparent depth at the frequency f = 387 Hz
ZST_1	m	centroid depth at the frequency f = 387 Hz
RHOA_2	Ωm	apparent resistivity at the frequency f = 1,821 Hz
KDA_2	m	apparent depth at the frequency f = 1,821 Hz
ZST_2	m	centroid depth at the frequency f = 1,821 Hz
RHOA_3	Ωm	apparent resistivity at the frequency f = 5,407 Hz
KDA_3	m	apparent depth at the frequency f = 5,407 Hz
ZST_3	m	centroid depth at the frequency f = 5,407 Hz
RHOA_4	Ωm	apparent resistivity at the frequency f = 8,395 Hz
KDA_4	m	apparent depth at the frequency f = 8,395 Hz
ZST_4	m	centroid depth at the frequency f = 8,395 Hz
RHOA_5	Ωm	apparent resistivity at the frequency f = 41,440 Hz
KDA_5	m	apparent depth at the frequency f = 41,440 Hz
ZST_5	m	centroid depth at the frequency f = 41,440 Hz
RHOA_6	Ωm	apparent resistivity at the frequency f = 133,300 Hz
KDA_6	m	apparent depth at the frequency f = 133,300 Hz
ZST_6	m	centroid depth at the frequency f = 133,300 Hz

4) Inversion models (five layers) HEM136_INV_L5.XYZ

Example

/Processing by A. Ullmann (BGR) using Oasis montaj

/GPS corrected (incl. TOPO_INV correction)

/ X Y LON LAT RECORD UTC TOPO H_RADAR H_LASER BIRD_NN H_BARO RHO_I_1 D_I_1 ... RHO_I_4 D_I_4 RHO_I_5 QAL

//Flight 13601

//Date 2009/08/26

Line 1.1

```
570960 5695534 4.020218 51.406585 77880 133744.0 -1.00 59.59 57.86 56.86 56.53 0.69 0.75 ... 0.35 1.76 1.64 11.09
570957 5695534 4.020176 51.406586 77881 133744.1 -1.01 58.82 57.09 56.09 55.91 0.97 0.73 ... 0.37 1.67 1.54 9.59
570954 5695534 4.020134 51.406587 77882 133744.2 -1.02 58.08 56.32 55.31 55.28 1.41 0.73 ... 0.78 0.94 1.29 8.67
```

In this data file all necessary position parameters and inversion models are stored in the order of the following description:

Channel	Unit	Remarks
X	m	UTM easting in m (WGS 84, Zone 31N), these coordinates have a false easting of 500000 metres
Y	m	UTM northing in m (WGS 84, Zone 31N), these coordinates have no false northing
LON	°	geographic longitude, reference system WGS 84
LAT	°	geographic latitude, reference system WGS 84
RECORD		time mark increasing by 1 every 0.1 seconds
UTC_TIME	hhmmss.s	GPS time (UTC)
TOPO	m	topographic elevation (in metres above sea level)
H_RADAR	m	smoothed value of the radar altitude minus the effective cable length from the helicopter to the bird, corresponds to the bird altitude
H_LASER	m	estimated value of the laser altitude, corresponds to the bird altitude
BIRD_NN	m	smoothed bird elevation (in metres above sea level), reference system: WGS84
H_BARO	m	smoothed value of the barometric sensor minus the effective cable length from the helicopter to the bird
RHO_I_1	Ωm	resistivity of the top layer of a five-layer inversion model
D_I_1	m	thickness of the top layer of a five-layer inversion model
RHO_I_2	Ωm	resistivity of the second layer of a five-layer inversion model
D_I_2	m	thickness of the second layer of a five-layer inversion model
RHO_I_3	Ωm	resistivity of the third layer of a five-layer inversion model
D_I_3	m	thickness of the third layer of a five-layer inversion model
RHO_I_4	Ωm	resistivity of the fourth layer of a five-layer inversion model
D_I_4	m	thickness of the fourth layer of a five-layer inversion model
RHO_I_5	Ωm	resistivity of the fifth layer of a five-layer inversion model
QALL	%	misfit of the inversion (L1 norm)

Remarks:

The header contains following additional lines:

/IFREQUENCY

/ 1 1 0 1 1 1

/NUMLAYER

/ 5

/MUELAYER

/ 0

5) Inversion models (fifteen layers) HEM136_INV_L15.XYZ

Example

/Processing by A. Ullmann (BGR) using Oasis montaj

/GPS corrected (incl. TOPO_INV correction)

/ X Y LON LAT RECORD UTC TOPO H_RADAR H_LASER BIRD_NN H_BARO RHO_I_1 D_I_1 ... RHO_I14 D_I14 RHO_I15 QALL

//Flight 13601

//Date 2009/08/26

Line 1.1

```
570960 5695534 4.020218 51.406585 77880 133744.0 -1.00 59.59 57.86 56.86 56.53 0.63 0.33 ... 0.53 0.53 1.80 14.74
570957 5695534 4.020176 51.406586 77881 133744.1 -1.01 58.82 57.09 56.09 55.91 0.65 0.36 ... 0.54 0.54 1.76 12.83
570954 5695534 4.020134 51.406587 77882 133744.2 -1.02 58.08 56.32 55.31 55.28 0.57 0.29 ... 0.53 0.57 1.45 13.09
```

In this data file all necessary position parameters and inversion models are stored in the order of the following description:

Channel	Unit	Remarks
X	m	UTM easting in m (WGS 84, Zone 31N), these coordinates have a false easting of 500000 metres
Y	m	UTM northing in m (WGS 84, Zone 31N), these coordinates have no false northing
LON	°	geographic longitude, reference system WGS 84
LAT	°	geographic latitude, reference system WGS 84
RECORD		time mark increasing by 1 every 0.1 seconds
UTC_TIME	hhmmss.s	GPS time (UTC)
TOPO	m	topographic elevation (in metres above sea level)
H_RADAR	m	smoothed value of the radar altitude minus the effective cable length from the helicopter to the bird, corresponds to the bird altitude
H_LASER	m	estimated value of the laser altitude, corresponds to the bird altitude
BIRD_NN	m	smoothed bird elevation (in metres above sea level), reference system: WGS84
H_BARO	m	smoothed value of the barometric sensor minus the effective cable length from the helicopter to the bird
RHO_I_1	Ωm	resistivity of the top layer of a fifteen-layer inversion model
D_I_1	m	thickness of the top layer of a fifteen-layer inversion model
...
...
RHO_I14	Ωm	resistivity of the fourteenth layer of a fifteen-layer inversion model
D_I14	m	thickness of the fourteenth layer of a fifteen-layer inversion model
RHO_I15	Ωm	resistivity of the fifteenth layer of a fifteen-layer inversion model
QALL	%	misfit of the inversion (L1 norm)

Remarks:

The header contains following additional lines:

/IFREQUENCY

/ 1 1 0 1 1 1

/NUMLAYER

/ 15

/MUELAYER

/ 0

B) Magnetics

Description of the ASCII coded data file **HMG136.XYZ** containing the final (levelled) data of a helicopter-borne magnetic (HMG) survey

```

/BGR HEADER:
/
/AREANAME
/PERKPOLDER
/AREACODE
/136
/C_MERIDIAN, ZONE and GEOID FOR X and Y
/ 3 31 WGS84
/ELLIPSOID FOR LON AND LAT
/WGS84
/DEVICE
/G-822A
/IGRF
/2005
/LON_BASE
/12.675
/LAT_BASE
/52.07167
/ALT_BASE
/78
/TOWCABLE
/ 40.0
/DUMMY
/ -9999
/PRIVTEXT
/Processing by M. Ibs-von Seht

```

Example:

```

/ X      Y      LON      LAT      RECORD      UTC_DATE      UTC_TIME      ALT_BIRD      H_RADAR_RAW      H_LASER_RAW      T_BASE_RAW      T_BASE_F      T_RAW      DELTA_T      DELTA_T_LEV
//Flight 13601
//Date 2009/08/26
Line 1.1
570960  5695534  4.020218  51.406585  77880  20090826  133744.0  52.0      316.7      0.0      49146.57  49146.57  48674.00  83.72      82.58
570957  5695534  4.020176  51.406586  77881  20090826  133744.1  51.2      314.9      0.0      49146.57  49146.57  48674.01  83.74      82.59
570954  5695534  4.020134  51.406587  77882  20090826  133744.2  50.5      313.0      0.0      49146.57  49146.57  48674.04  83.75      82.61

```


In this data file all necessary position parameters and magnetic data are stored in the order of the following description:

Channel	Unit	Remarks
X	m	UTM easting in m (WGS 84, Zone 31N), these coordinates have a false easting of 500000 metres
Y	m	UTM northing in m (WGS 84, Zone 31N), these coordinates have no false northing
LON	°	geographic longitude, reference system WGS 84
LAT	°	geographic latitude, reference system WGS 84
RECORD		time mark increasing by 1 every 0.1 seconds
UTC_DATE	yyyymmdd	date
UTC_TIME	hhmmss.s	GPS time (UTC)
ALT_BIRD	m	smoothed bird elevation (in metres above sea level), reference system: WGS84
H_RADAR_RAW	ft	value of the radar altimeter (helicopter altitude)
H_LASER_RAW	m	value of the laser altimeter (bird altitude)
T_BASE_RAW	nT	raw data of the magnetic field at the base station
T_BASE_F	nT	processed data of the magnetic field at the base station
T_RAW	nT	raw data of the magnetic field at the bird
DELTA_T	nT	anomalies of the magnetic field
DELTA_T_LEV	nT	levelled anomalies of the magnetic field

Remarks:

Lines starting with "/" comment,
 Lines starting with "/" flight number and date,
 Lines starting with "Line" lines,
 Lines starting with "Tie" tie lines.

C) Radiometry

Description of the ASCII coded data file **HRD136.XYZ** containing the final (levelled) data of a helicopter-borne radiometric (HRD) survey

```

/BGR HEADER:
/
/AREANAME
/PERKPOLDER
/AREACODE
/136
/C_MERIDIAN, ZONE and GEOID FOR X AND Y
/ 3 31 WGS84
/ELLIPSOID FOR LON AND LAT
/WGS84
/DEVICE
/GR-820
/BACKGROUND (IAEA 2003, S.60) a(TC), b(TC), a(K), b(K), a(U), b(U), a(Th), b(Th), a(upU), b(upU)
/31.09, 0.7224, 5.51, 0.0405, 0.48, 0.0326, 0.33, 0.0412, 0.0, 0.0090
/STRIPPING (IAEA 2003, S.65) alpha, beta, gamma
/0.2485, 0.3852, 0.6599
/ATTENUATION (IAEA 2003, S.67) mue(TC), mue(K), mue(U), mue(Th)
/-0.006468, -0.007733, -0.008132, -0.005784
/SENSITIVITY (IAEA 2003, S.68) S(K), S(U), S(Th)
/28.42, 2.916, 1.962
/TOWCABLE
/ 40.00
/DUMMY
/-9999
/PRIVTEXT
/Processing by M. Ibs-von Seht
Example:
/ X      Y      LON      LAT      RECORD      UTC_DATE      UTC_TIME      ALT_BIRD      H_RADAR_RAW      HAG      PRESSURE      TEMP      LIVE_T      COSMIC_RAW      TOT_RAW      POT_RAW      URA_RAW      THO_RAW      URAUP_RAW
Continuation of last line:
      TOT      POT      URA      THO      TOT_LEV      POT_LEV      URA_LEV      THO_LEV      EXPO
//Flight 13601
//Date 2009/08/26
Line 1.1
570960 5695534 4.020218 51.406585 77880 20090826 133744.0 52.0      316.7 100.1 100.942 23.2 936 64 102 7 6 6 0
570931 5695535 4.019799 51.406594 77890 20090826 133745.0 44.4      294.3 93.0 101.027 23.2 953 73 111 6 6 2 1
570901 5695535 4.019377 51.406597 77900 20090826 133746.0 38.2      274.8 86.8 101.101 23.2 945 52 93 11 8 1 2
Continuation of last three lines:
      30.7 -0.03 0.74 0.22 30.90 0.00 0.60 0.24 0.46
      37.3 0.05 0.56 0.13 37.38 0.05 0.42 0.15 0.39
      18.0 -0.02 0.94 0.03 17.87 0.00 0.79 0.05 0.53

```

In this data file all necessary position parameters and radiometric data are stored in the order of the following description:

Channel	Unit	Remarks
X	m	UTM easting in m (WGS 84, Zone 31N), these coordinates have a false easting of 500000 metres
Y	m	UTM northing in m (WGS 84, Zone 31N), these coordinates have no false northing
LON	°	geographic longitude, reference system WGS 84
LAT	°	geographic latitude, reference system WGS 84
RECORD		time mark increasing by 1 every 0.1 seconds
UTC_DATE	yyyymmdd	date
UTC_TIME	hhmmss.s	GPS time (UTC)
ALT_BIRD	m	smoothed bird elevation (in metres above sea level), reference system: WGS84
H_RADAR_RAW	ft	value of the radar altimeter
HAG	m	altitude of helicopter above ground level
PRESSURE	kPa	air pressure
TEMP	°C	air temperature
LIVE_T	ms	live time
COSMIC	cps	cosmic radiation > 3 MeV
TOT_RAW	cps	measured total count rate
POT_RAW	cps	measured potassium count rate
URA_RAW	cps	measured uranium count rate
THO_RAW	cps	measured thorium count rate
URAUP_RAW	cps	measured uranium count rate in upward looking crystal
TOT	cps	total count
POT	%	potassium concentration on ground level
URA	ppm	equivalent uranium concentration ground level
THO	ppm	equivalent thorium concentration ground level
TOT_LEV	cps	levelled total count
POT_LEV	%	levelled potassium concentration on ground level
URA_LEV	ppm	levelled equivalent uranium concentration on ground level
THO_LEV	ppm	levelled equivalent thorium concentration on ground level
EXPO	µR/h	ground level exposure rate

Remarks:

Lines starting with "/" comment,
 Lines starting with "//" flight number and date,
 Lines starting with "Line" lines,
 Lines starting with "Tie" tie lines.

Appendix III

DVD

<ul style="list-style-type: none"> \Acrobat Reader\ <ul style="list-style-type: none"> \Acrobat Reader\Adobe - Adobe Reader herunterladen.URL \Linux\ <ul style="list-style-type: none"> AdbeRdr9.3.4-1_i486linux_deu.bin \Mac\ <ul style="list-style-type: none"> AdbeRdr930_de_DE_i386.pkg.zip \Windows\ <ul style="list-style-type: none"> AdbeRdr934_de_DE.exe \Data\ <ul style="list-style-type: none"> \HEM\ <ul style="list-style-type: none"> Format_description_HEM136.txt HEM136_APP.xyz HEM136_DAT.xyz HEM136_INV_L15.xyz HEM136_INV_L5.xyz HEM136_RAW.xyz \HMG\ <ul style="list-style-type: none"> Format_description_HMG136.txt HMG136.XYZ \HRD\ <ul style="list-style-type: none"> Format_description_HRD136.txt HRD136.XYZ \Maps\ <ul style="list-style-type: none"> \ArcGis\ <ul style="list-style-type: none"> 136 Perkpolder apparent resistivity rhoa1.mxd 136 Perkpolder apparent resistivity rhoa2.mxd 136 Perkpolder apparent resistivity rhoa3.mxd 136 Perkpolder apparent resistivity rhoa4.mxd 136 Perkpolder apparent resistivity rhoa5.mxd 136 Perkpolder apparent resistivity rhoa6.mxd 136 Perkpolder centroid depth zst1.mxd 136 Perkpolder centroid depth zst2.mxd 136 Perkpolder centroid depth zst3.mxd 136 Perkpolder centroid depth zst4.mxd 136 Perkpolder centroid depth zst5.mxd 136 Perkpolder centroid depth zst6.mxd 136 Perkpolder DEM.mxd 136 Perkpolder Depth to saltwater.mxd 136 Perkpolder Exposure Rate.mxd 136 Perkpolder flight lines.mxd 136 Perkpolder Magnetic Anomalies.mxd 136 Perkpolder Potassium.mxd 136 Perkpolder resistivity -01m.mxd 136 Perkpolder resistivity -02m.mxd 136 Perkpolder resistivity -04m.mxd 136 Perkpolder resistivity -07m.mxd 136 Perkpolder resistivity -10m.mxd 136 Perkpolder resistivity -13m.mxd 136 Perkpolder resistivity -16m.mxd 136 Perkpolder resistivity -20m.mxd 136 Perkpolder Thorium.mxd 136 Perkpolder Total count.mxd 136 Perkpolder Uranium.mxd \ArcGis\Legends\ <ul style="list-style-type: none"> 136 Perkpolder Legende apparent resistivity rhoa1.bmp 136 Perkpolder Legende apparent resistivity rhoa2.bmp 136 Perkpolder Legende apparent resistivity rhoa3.bmp 136 Perkpolder Legende apparent resistivity rhoa4.bmp 136 Perkpolder Legende apparent resistivity rhoa5.bmp 136 Perkpolder Legende apparent resistivity rhoa6.bmp 	<ul style="list-style-type: none"> 136 Perkpolder Legende centroid depth zst1.bmp 136 Perkpolder Legende centroid depth zst2.bmp 136 Perkpolder Legende centroid depth zst3.bmp 136 Perkpolder Legende centroid depth zst4.bmp 136 Perkpolder Legende centroid depth zst5.bmp 136 Perkpolder Legende centroid depth zst6.bmp 136 Perkpolder Legende DEM.bmp 136 Perkpolder Legende Depth to saltwater.bmp 136 Perkpolder Legende Exposure Rate.bmp 136 Perkpolder Legende flight lines.bmp 136 Perkpolder Legende Magnetic anomalies.bmp 136 Perkpolder Legende Potassium.bmp 136 Perkpolder Legende resistivity -01m.bmp 136 Perkpolder Legende resistivity -02m.bmp 136 Perkpolder Legende resistivity -04m.bmp 136 Perkpolder Legende resistivity -07m.bmp 136 Perkpolder Legende resistivity -10m.bmp 136 Perkpolder Legende resistivity -13m.bmp 136 Perkpolder Legende resistivity -16m.bmp 136 Perkpolder Legende resistivity -20m.bmp 136 Perkpolder Legende Thorium.bmp 136 Perkpolder Legende Total count.bmp 136 Perkpolder Legende Uranium.bmp <ul style="list-style-type: none"> \ArcGis\Oasis\ <ul style="list-style-type: none"> 136_rho_01mbsl.map 136_rho_01mbsl.map.xml 136_rho_02mbsl.map 136_rho_02mbsl.map.xml 136_rho_04mbsl.map 136_rho_04mbsl.map.xml 136_rho_07mbsl.map 136_rho_07mbsl.map.xml 136_rho_10mbsl.map 136_rho_10mbsl.map.xml 136_rho_13mbsl.map 136_rho_13mbsl.map.xml 136_rho_16mbsl.map 136_rho_16mbsl.map.xml 136_rho_20mbsl.map 136_rho_20mbsl.map.xml 136_saltwaterdepth.map 136_saltwaterdepth.map.xml da1_fin.GRD da1_fin.GRD.gi da1_fin.GRD.xml da1_fin.map da1_fin.map.xml da2_fin.GRD da2_fin.GRD.gi da2_fin.GRD.xml da2_fin.map da2_fin.map.xml da3_fin.GRD da3_fin.GRD.gi da3_fin.GRD.xml da3_fin.map da3_fin.map.xml da4_fin.GRD da4_fin.GRD.gi da4_fin.GRD.xml da4_fin.map da4_fin.map.xml
--	--

da5_fin.GRD
da5_fin.GRD.gi
da5_fin.GRD.xml
da5_fin.map
da5_fin.map.xml
da6_fin.GRD
da6_fin.GRD.gi
da6_fin.GRD.xml
da6_fin.map
da6_fin.map.xml
EXPO.grd
EXPO.grd.gi
EXPO.grd.xml
MAG_error.grd
MAG_error.grd.gi
MAG_error.grd.xml
MAG_LEV.grd
MAG_LEV.grd.gi
MAG_LEV.grd.xml
map01.map
map01.map.xml
map01.mdf
map-hrd.map
map-hrd.map.xml
map-hrd.mdf
POT_error.grd
POT_error.grd.gi
POT_error.grd.xml
POT_l.grd
POT_l.grd.gi
POT_l.grd.xml
POT_LEV.grd
POT_LEV.grd.gi
POT_LEV.grd.xml
rho_010dmbsl.grd
rho_010dmbsl.grd.gi
rho_010dmbsl.grd.xml
rho_020dmbsl.grd
rho_020dmbsl.grd.gi
rho_020dmbsl.grd.xml
rho_040dmbsl.grd
rho_040dmbsl.grd.gi
rho_040dmbsl.grd.xml
rho_070dmbsl.grd
rho_070dmbsl.grd.gi
rho_070dmbsl.grd.xml
rho_100dmbsl.grd
rho_100dmbsl.grd.gi
rho_100dmbsl.grd.xml
rho_130dmbsl.grd
rho_130dmbsl.grd.gi
rho_130dmbsl.grd.xml
rho_160dmbsl_ply.GRD
rho_160dmbsl_ply.GRD.gi
rho_160dmbsl_ply.GRD.xml
rho_200dmbsl_ply.GRD
rho_200dmbsl_ply.GRD.gi
rho_200dmbsl_ply.GRD.xml
rhoa1_fin.GRD
rhoa1_fin.GRD.gi
rhoa1_fin.GRD.xml
rhoa1_fin.map
rhoa2_fin.GRD
rhoa2_fin.GRD.gi
rhoa2_fin.GRD.xml
rhoa2_fin.map
rhoa2_fin.map.xml
rhoa3_fin.GRD
rhoa3_fin.GRD.gi
rhoa3_fin.GRD.xml

rhoa3_fin.map
rhoa3_fin.map.xml
rhoa4_fin.GRD
rhoa4_fin.GRD.gi
rhoa4_fin.GRD.xml
rhoa4_fin.map
rhoa4_fin.map.xml
rhoa5_fin.GRD
rhoa5_fin.GRD.gi
rhoa5_fin.GRD.xml
rhoa5_fin.map
rhoa5_fin.map.xml
rhoa6_fin.GRD
rhoa6_fin.GRD.gi
rhoa6_fin.GRD.xml
rhoa6_fin.map
rhoa6_fin.map.xml
THO_error.grd
THO_error.grd.gi
THO_error.grd.xml
THO_l.grd
THO_l.grd.gi
THO_l.grd.xml
THO_LEV.grd
THO_LEV.grd.gi
THO_LEV.grd.xml
TOT_error.grd
TOT_error.grd.gi
TOT_error.grd.xml
TOT_l.grd
TOT_l.grd.gi
TOT_l.grd.xml
TOT_LEV.grd
TOT_LEV.grd.gi
TOT_LEV.grd.xml
URA_error.grd
URA_error.grd.gi
URA_error.grd.xml
URA_l.grd
URA_l.grd.gi
URA_l.grd.xml
URA_LEV.grd
URA_LEV.grd.gi
URA_LEV.grd.xml
zst1_fin.GRD
zst1_fin.GRD.gi
zst1_fin.GRD.xml
zst1_fin.map
zst1_fin.map.xml
zst2_fin.GRD
zst2_fin.GRD.gi
zst2_fin.GRD.xml
zst2_fin.map
zst2_fin.map.xml
zst3_fin.GRD
zst3_fin.GRD.gi
zst3_fin.GRD.xml
zst3_fin.map
zst3_fin.map.xml
zst4_fin.GRD
zst4_fin.GRD.gi
zst4_fin.GRD.xml
zst4_fin.map
zst4_fin.map.xml
zst5_fin.GRD
zst5_fin.GRD.gi
zst5_fin.GRD.xml
zst5_fin.map
zst5_fin.map.xml
zst6_fin.GRD

zst6_fin.GRD.gi	UI_1360049.PDF
zst6_fin.GRD.xml	UI_1360051.PDF
zst6_fin.map	UI_1360059.PDF
zst6_fin.map.xml	UI_1360061.PDF
\ArcGis\Topography\ 136_Perkpolder_flightlines.tfw	UI_1360069.PDF
136_Perkpolder_flightlines.tif	UI_1360071.PDF
136 Perkpolder Niederlande ÜK.pdf	UI_1360079.PDF
136 Perkpolder Niederlande ÜK.png	UI_1360081.PDF
Project_49c.img	UI_1360089.PDF
Project_49c.img.vat.dbf	UI_1360091.PDF
Project_49c.rrd	UI_1360099.PDF
Project_55a.img	UI_1360101.PDF
Project_55a.img.vat.dbf	UI_1360109.PDF
Project_55a.rrd	UI_1360111.PDF
Project_65h.img	UI_1360119.PDF
Project_65h.img.vat.dbf	UI_1360121.PDF
Project_65h.rrd	UI_1360129.PDF
project_67f11.img	UI_1360131.PDF
project_67f11.img.vat.dbf	UI_1360139.PDF
project_67f11.rrd	UI_1360141.PDF
\DEM\ 136 Perkpolder DEM.pdf	UI_1360151.PDF
\Flightlines\ 136 Perkpolder flight lines.pdf	UI_1360161.PDF
\HEM\ 136 Perkpolder apparent resistivity rhoa1.pdf	UI_1360171.PDF
136 Perkpolder apparent resistivity rhoa2.pdf	UI_1360181.PDF
136 Perkpolder apparent resistivity rhoa3.pdf	UI_1360191.PDF
136 Perkpolder apparent resistivity rhoa4.pdf	UI_1360201.PDF
136 Perkpolder apparent resistivity rhoa5.pdf	UI_1360211.PDF
136 Perkpolder apparent resistivity rhoa6.pdf	UI_1360221.PDF
136 Perkpolder centroid depth zst1.pdf	\L5\ UI_1360011.PDF
136 Perkpolder centroid depth zst2.pdf	UI_1360019.PDF
136 Perkpolder centroid depth zst3.pdf	UI_1360021.PDF
136 Perkpolder centroid depth zst4.pdf	UI_1360029.PDF
136 Perkpolder centroid depth zst5.pdf	UI_1360031.PDF
136 Perkpolder centroid depth zst6.pdf	UI_1360039.PDF
136 Perkpolder Depth to saltwater.pdf	UI_1360041.PDF
136 Perkpolder resistivity -01m.pdf	UI_1360049.PDF
136 Perkpolder resistivity -02m.pdf	UI_1360051.PDF
136 Perkpolder resistivity -04m.pdf	UI_1360059.PDF
136 Perkpolder resistivity -07m.pdf	UI_1360061.PDF
136 Perkpolder resistivity -10m.pdf	UI_1360069.PDF
136 Perkpolder resistivity -13m.pdf	UI_1360071.PDF
136 Perkpolder resistivity -16m.pdf	UI_1360079.PDF
136 Perkpolder resistivity -20m.pdf	UI_1360081.PDF
\HMG\ 136 Perkpolder Magnetic Anomalies.pdf	UI_1360089.PDF
\HRD\ 136 Perkpolder Exposure Rate.pdf	UI_1360091.PDF
136 Perkpolder Potassium.pdf	UI_1360099.PDF
136 Perkpolder Thorium.pdf	UI_1360101.PDF
136 Perkpolder Total count.pdf	UI_1360109.PDF
136 Perkpolder Uranium.pdf	UI_1360111.PDF
\Report\ Technical Report CLIWAT 136 Perkpolder.pdf	UI_1360119.PDF
\Vertical sections\ \L15\ UI_1360011.PDF	UI_1360121.PDF
UI_1360019.PDF	UI_1360129.PDF
UI_1360021.PDF	UI_1360131.PDF
UI_1360029.PDF	UI_1360139.PDF
UI_1360031.PDF	UI_1360141.PDF
UI_1360039.PDF	UI_1360151.PDF
UI_1360041.PDF	UI_1360161.PDF
	UI_1360171.PDF
	UI_1360181.PDF
	UI_1360191.PDF
	UI_1360201.PDF
	UI_1360211.PDF
	UI_1360221.PDF

Appendix IV

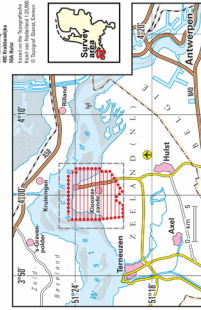
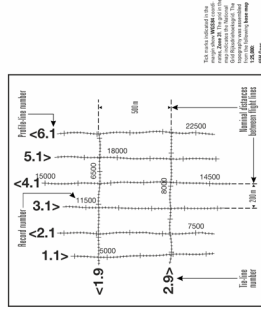
Maps

(reduced to a scale of 1:75,000)

CLIWAT – Adaptive and sustainable water
management and protection of society
and nature in an extreme climate

**AIRBORNE GEOPHYSICAL SURVEY
PERKPOLDER / THE NETHERLANDS**

FLIGHT LINES



Scale 1:25 000 (4 cm \equiv 1 km)

BGR	Federal Institute for Geosciences and Natural Resources (BGR) Hannover, Federal Republic of Germany
DTU	DTU The Netherlands
DELTA	Deltares The Netherlands
EU	The project is co-financed by the European Union
Area:	Perkpolder (The Netherlands)
Parameter:	Topography and flight lines
Field campaign and processing:	August 2009 Mariusz Blichowski, Ingeborg Krawinkel, Jeroen Buijze, Wolfgang Volk, Michael Schabel (Writing/Mapping Service GmbH)
B.2.1. Geophysical Exploration – Technical Mineralogy:	Airborne Geophysics Hannover 2011 - www.bgr.bund.de - halle@bgr.de



Alle anderen Karten und Vertikal-
sektionen sind in dieser Web-Fassung
des Berichtes nicht enthalten.

All other maps and vertical
resistivity sections are not included
in this web edition of the report.